Bachelor of Science Thesis in Electrical Engineering
Department of Electrical Engineering, Linköping University, 2018

Design of Bidirectional DC/DC Battery Management System for Electrical Yacht

Daniel Celius Zacharek and Filip Sundqvist

Bachelor of Science Thesis in Electrical Engineering

Design of Bidirectional DC/DC Battery Management System for Electrical Yacht

Daniel Celius Zacharek and Filip Sundqvist

LiTH-ISY-EX-ET--18/0475--SE

Supervisor:
Tomas Uno Jonsson
ISY, Linköping University

Examiner:
Mark Vesterbacka
ISY, Linköping University

Division of Integrated Circuits and Systems
Department of Electrical Engineering
Linköping University
SE-581 83 Linköping, Sweden

Abstract

Electrical vehicles are getting more popular as the technology around batteries and electrical motors are catching up to the more common combustion engines. Electrical boats are no exception but there are still a lot of boats using old combustion engines that have a big impact on the environment. This study aims to deepen the understanding of the integration of electrical motors into boats by proposing a design of a system using a bidirectional synchronous buck-boost converter. This converter is designed to handle the power transfer in a dual battery application, namely consisting of a 12 V battery and a 48 V battery. The converter includes proposed components, a PCB design, as well as the software that is required for the control of the power transfer. The results show that the converter design meets specification and, when using a test-bench, the software is capable of controlling the converter to achieve constant current and constant voltage in both directions.

Acknowledgement

We would like to thank the following people for their support given during our thesis work. Our supervisor, Tomas Uno Jonsson, for proposing this thesis subject and for his valuable feedback during this project, as well as his unwavering enthusiasm during our cooperation. Mark Vesterbacka, our examiner, for his response on our report and presentation. Our opponents Hassan Moumin and Faris Al-Egli for reviewing the report and providing us with comments and bringing a discussion during the presentation.

Table of Contents

List of Figures

List of Tables

Table of Abbreviations

Table 1-1 Table of Abbreviations

Acronym	Meaning
DC	Direct Current
BLDC	Brushless Direct Current Motor
PCB	Printed Circuit Board
PWM	Pulse Width Modulation
PV	Photovoltaic
MPPT	Maximum Power Point Tracking
MOSFET	Metal Oxide Semiconductor Field Effect Transistor
AC	Alternating Current
SMD	Surface Mounted Device
SoC	State of Charge
DoD	Depth of Discharge
BMS	Battery Management System
IC	Integrated Circuit
ZVS	Zero Voltage Switching
RMS	Root Mean Square
MLCC	Multi-Layer Ceramic Capacitor
PI	Proportional Integral

1 Introduction

Today the transportation industry is expanding with electric vehicles, but the evolution of electrical boats and yachts is going much slower. In order to change this trend a project about updating a yacht from having a fossil fueled petrol engine to a brushless dc-motor (BLDC) powered by PV panels and regenerative braking is proposed at Linköping University. By designing a bidirectional buck-boost converter for a dual battery system the goal is to allow power flow between batteries to minimize the need for battery charging.

1.1 Background

A campaign has been proposed by the current Swedish government that will subsidize replacing combustion engines with electrical motors hoping to spur many into purchasing an electrical motor. This campaign is motivated by environmental reasons such as that older combustion engines release large amounts of hydrocarbons [1].

The electrical system of a yacht, which in most cases run on 12 V batteries, can be difficult to integrate with an electrical motor system that might use a different voltage or higher current. At the time of writing there are a few commercially dedicated solutions to replace an old engine with an electrical motor to update the system. Design of a system for this purpose can be valuable experience when it comes to future implementations.

The proposed system layout is that the yacht, a 30 feet Comfort will be equipped with two different PV panels, one horizontal in the front and one with flexible movement in the rear. The energy storage on the yacht consists of a 12 V lead-acid battery and a 48 V LiFePo battery. The 12 V battery is charged by the PV panels, which supplies power to the equipment on the yacht while the 48 V battery is connected to the motor that can both consume and generate energy while sailing. The two batteries are connected by the bidirectional DC/DC converter to allow transfer of energy in both directions, a block diagram of the system is shown in Figure 1-1. The system uses an Arduino Due to provide a battery management system (BMS) that controls the power flow and makes sure that the batteries are not over-charged or too deeply discharged. The idea of the BMS is to allow more control of the power generated by the PV panels and the motor with the goal to provide energy for the yacht to run at 5 knots for about an hour every day which corresponds to about 1.33 kWh consumption.

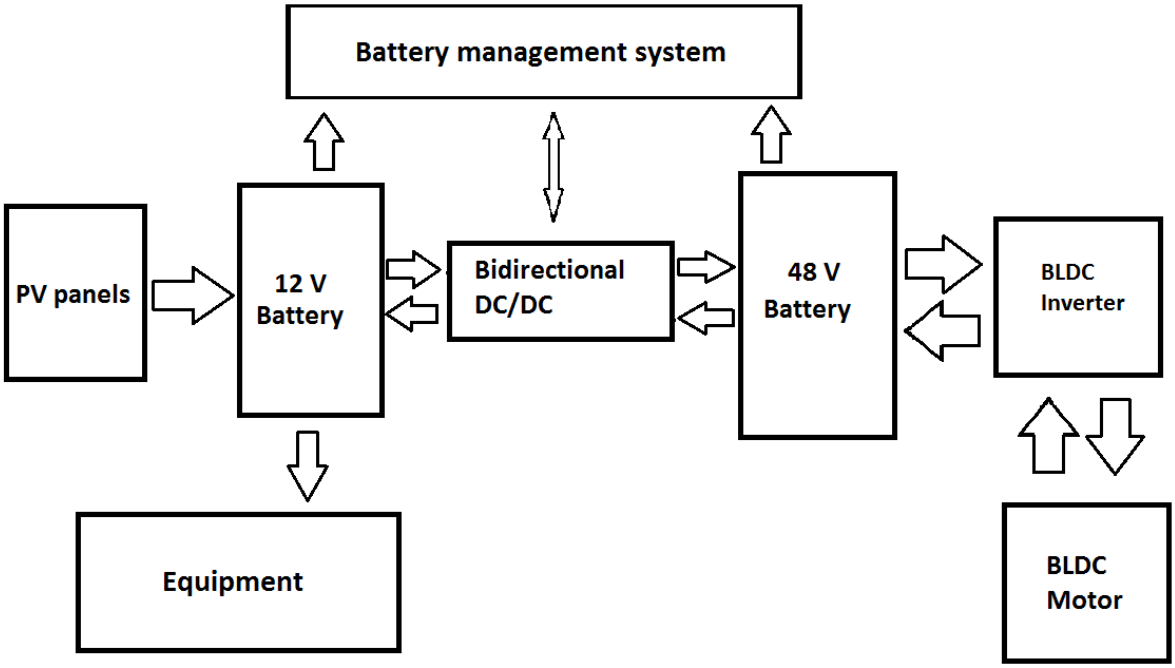

Figure 1-1 Block diagram of the system

1.2 Motivation and Purpose

At present, there is a lack of broad knowledge and experience with systems using multiple different batteries. Therefore, the motivation of this report is to increase knowledge about converters and energy transfer strategies, specifically by studying, designing and simulating a system using two batteries optimized for naval use.

The purpose of the project is to design a bidirectional DC/DC converter to implement the function of controlling the energy transfer between the batteries. In order to succeed with the energy transfer, an understanding of how the system shall be interconnected with the BLDC-motor and the PV panels is required. For this interconnection, a design using a shared PCB for the bidirectional DC/DC converter and the BLDC-inverter is proposed to increase the energy density. Software shall also be implemented on an Arduino Due which controls the power transfer and supervises the batteries. This design will provide broader insight on the techniques that can be used to increase the days at sea without land charging with a dual battery setup and hopefully inspire others to convert their boat into a greener solution.

1.3 Questions and Problems

The report aims towards answering the following questions:

- How can a bidirectional converter for a dual battery system be designed?
- How can the bidirectional converter design be implemented on a PCB?
- How can software be implemented to control the power transfer of the system?
- How should the software decide when to transfer energy?

With these questions in mind, a suitable method is chosen. The design of the implementation is decided after simulations of the system. Suggestions for components and thermal management is provided. Finally, the software will be evaluated using a test-bench.

1.4 Limitations

There are multiple limitations in this project that might affect the result which must be taken into consideration. First of all, the project time is limited to ten weeks. This means in turn that some design considerations may be shifted towards simplicity rather than efficiency. Since the project is funded by a single individual, money and component suppliers are also limitations. The electronics suppliers are Elfa Distrelec and Mouser. This will limit the choice of components and increase the importance of thorough simulations placing orders to not waste money. A third limitation is that the other parts of the system (presented in chapter 3.1.1) need to work in tandem with our design. Hence these components impact on the whole system must be considered. Special care is needed since the system is implemented on the same PCB as the circuit controlling the BLDC motor. The last limitation is the complexity of the software. It must be able to run on an Arduino Due which is limited in computing power.

2 Theory

The theory will address the underlying knowledge required with regards to DC/DC converters and batteries. It aims towards providing a base for the design choices in the method using previous experience in the field. Since power electronics has a long history of development, only some of the basics will be covered regarding DC/DC converters, thermal considerations and pulse width modulation (PWM). An important part of the converter is the use of transistors and inductors. To understand the operation of photovoltaic (PV) panels and driver circuits, the basics of their operation is explained.

2.1 DC/DC Converters and PWM

Power converters are an integral part of many electrical systems that require energy transfer between one voltage level to another, as the voltage required may be different to the voltage supplied. To achieve energy-efficient conversions, switch-mode conversion is used [2]. The three generic switch-mode DC/DC converters that will be explained are Buck, Boost and Buck-Boost DC/DC converters as well as the PWM required to control them. The theory and equations for PWM and generic switch mode converters are provided by [2] while the theory for the bidirectional buck-boost converter is provided by [3].

2.1.1 Pulse Width Modulation

Pulse-width modulation (PWM) is used to control the output voltage of DC/DC converters by controlling the on and off state of the switch/switches. As the name implies the width of a pulse is controlled by varying the time the pulse is "on" in relation to the switching period. This ratio between the time the switch is in the "on" position t_{on} and the switching period T_s, is called the duty cycle. Where the duty cycle can be expressed as

$$D = \frac{t_{on}}{T_s} \qquad (2\text{-}1)$$

Figure 2-1 a) shows a basic switch-mode DC/DC converter and Figure 2-1 b) illustrates how PWM can be implemented to control a switch with a certain duty cycle that determines the average output voltage v_o even though the input voltage and output load may fluctuate.

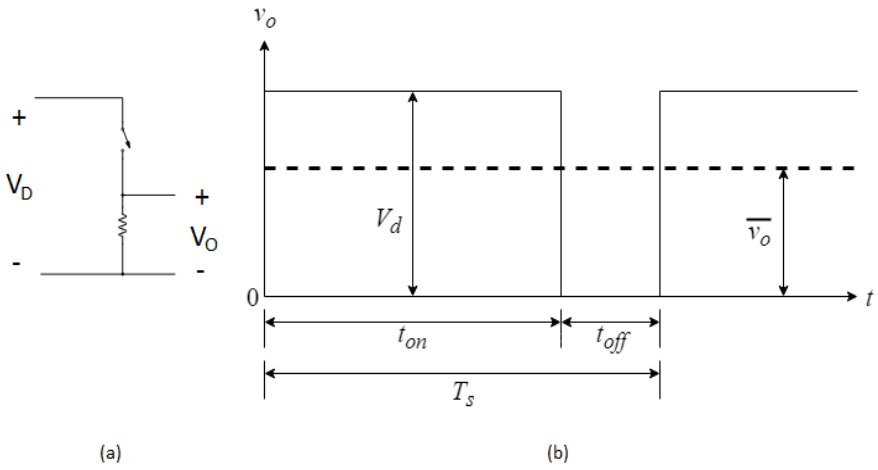

Figure 2-1 a) Switch-mode DC/DC conversion

By comparing a control voltage with a repetitive signal with a constant peak, a switch control signal with a duty cycle that will achieve the desired output voltage can be generated from a PWM. Generally, the control signal is the difference between the actual and desired output voltage and the repetitive signal is a sawtooth signal where its frequency determines the switching frequency. The relation between the duty cycle, control voltage and peak of the sawtooth signal can be described as

$$D = \frac{t_{on}}{T_s} = \frac{v_{control}}{\hat{V}_{st}}. \qquad (2\text{-}2)$$

where $v_{control}$ is the control voltage and $\hat{V}_{st}$is the peak of the sawtooth waveform, which can be seen in Figure 2-2.

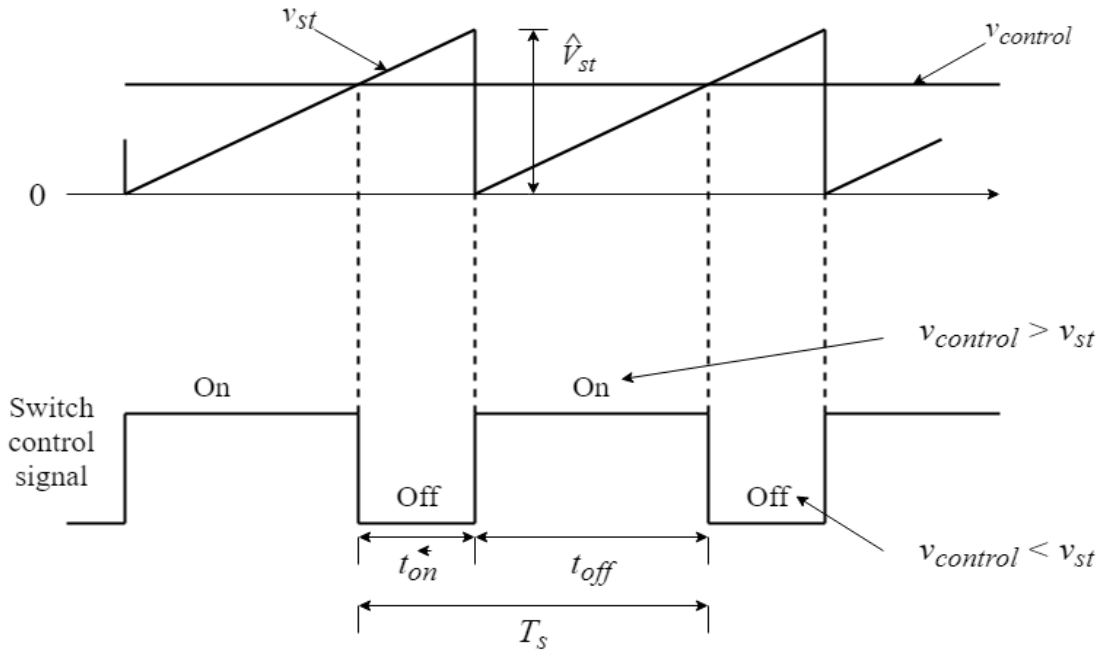

Figure 2-2 PWM

2.1.2 Generic switch mode converters

All of the converters that will be explained consist of a switching power-pole shown in Figure 2-3a. By changing the position of the bi-positional switch at a high frequency (using for example a PWM signal) the output voltage is turned into high frequency voltage pulses as shown by Va in Figure 2-3b).

By controlling the pulse width that determines what position the bi-directional switch is in, control over the averaged voltage output is allowed as shown by v_A in Figure 2-3b. The value of v_A is determined by

$$v_A = \frac{T_{up}}{T_s} V_{in} = d_A V_{in} \qquad 0 \leq d_A \leq 1 \qquad (2\text{-}3)$$

where d_A is the duty cycle.

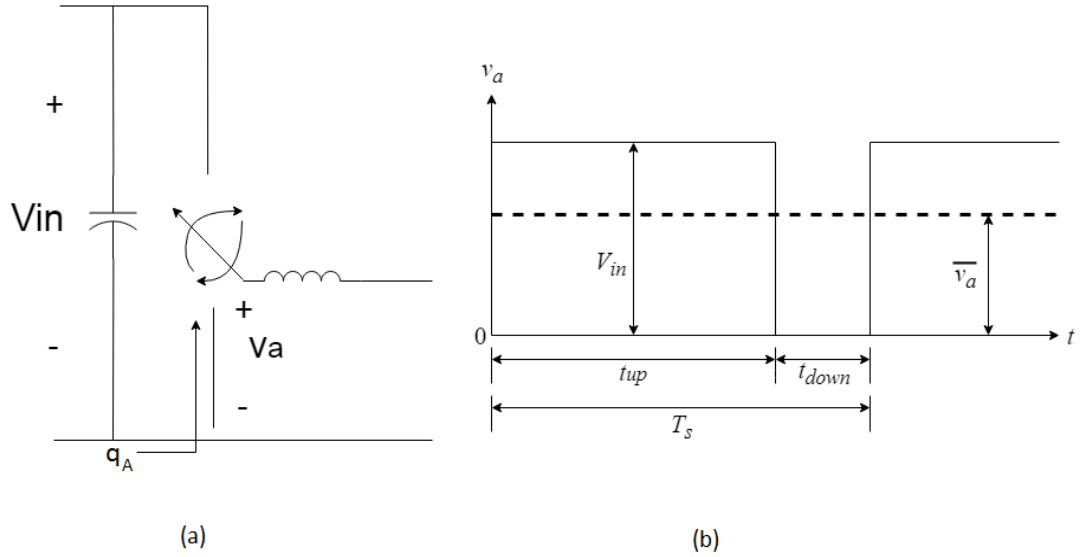

Figure 2-3 Switching power-pole as the building block

As can be seen in Figure 2-4a, the bi-positional switch in a switching power-pole can be realized using a transistor and a diode. This circuit is the basic building block for other converters. By placing an inductor in series with the current output of the transistor, a means of energy transfer from input to output is achieved. When the transistor is conducting the energy in the inductor increases drawn from the input source. When the transistor is blocking the energy in the inductor is transferred to the load. The inductor also filters the current as can be seen in Figure 2-4b.

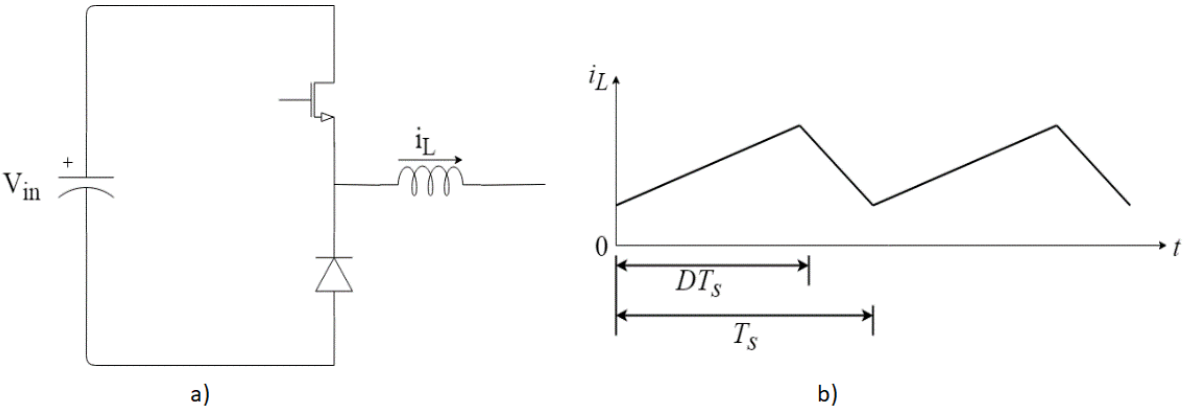

Figure 2-4 Switching power-pole

The Buck DC/DC converter is used as a step-down converter. Step-down means that the input voltage is converted to a lower output voltage. A circuit diagram of a Buck DC/DC converter can be seen in Figure 2-5. The voltage relation is given as

$$V_{OUT} = D \cdot V_{IN} \tag{2-4}$$

where D is the duty cycle, Vout is the output voltage and Vin is the input voltage.

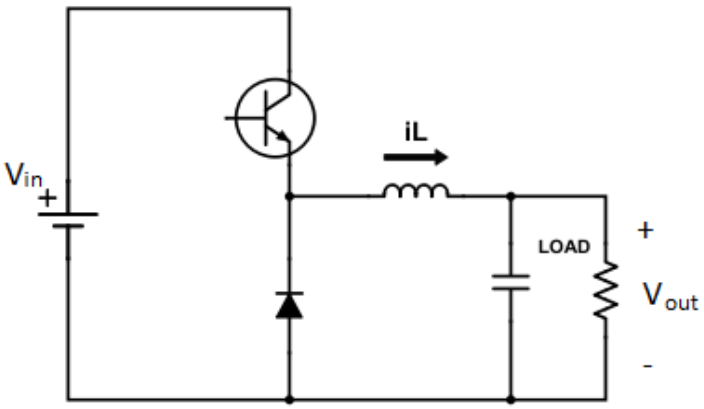

Figure 2-5 Buck circuit

The Boost DC/DC converter is used as a step-up converter. Steap-up means that the input voltage is converted to a higher output voltage. The circuit diagram of a Boost DC/DC converter can be seen in Figure 2-6. The output voltage is given by

$$V_{OUT} = \frac{V_{IN}}{(1-D)}. \tag{2-5}$$

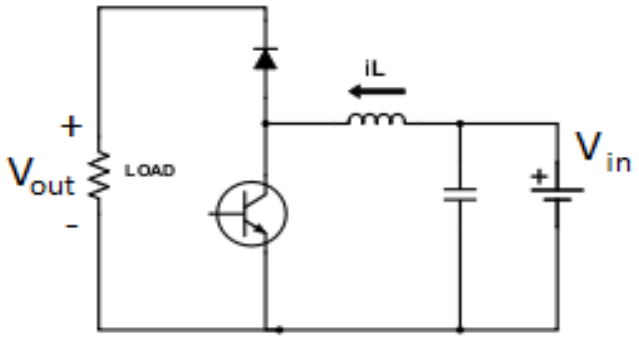

Figure 2-6 Boost circuit

The Buck-Boost DC/DC converter is used as both a step-down and a step-up converter, meaning that the input voltage can be converted to either a lower or a higher output voltage, however the single switch and diode limits the current to flow in one direction only. The circuit for an inverting buck-boost DC/DC converter can be seen in Figure 2-7. The relation between the input voltage, output voltage and duty cycle is the following

$$\frac{V_{OUT}}{V_{IN}} = \frac{D}{(1-D)} \tag{2-6}$$

where D is the duty cycle, Vout is the output voltage and Vin is the input voltage. By controlling the duty cycle the output voltage Vout can be both higher and lower.

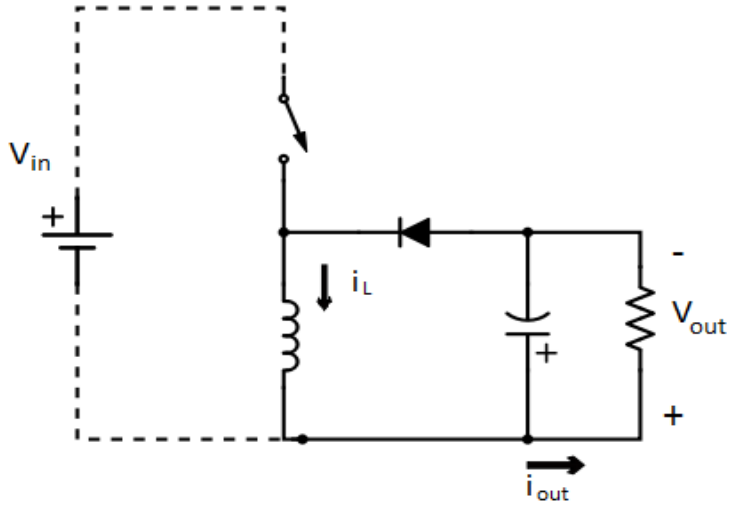

Figure 2-7 An inverting buck-boost circuit

The synchronous bidirectional half-bridge buck-boost converter differs from the generic buck-boost converter in that the output is not inverted and allows power to flow in both directions. Being synchronous means that the duty cycle for the both switches are complimentary, once one switch is conducting the other is blocking and vice versa. It is composed of two transistors with anti-parallel diodes, an inductor and can have filtering capacitors at each end, which can be seen in Figure 2-8.

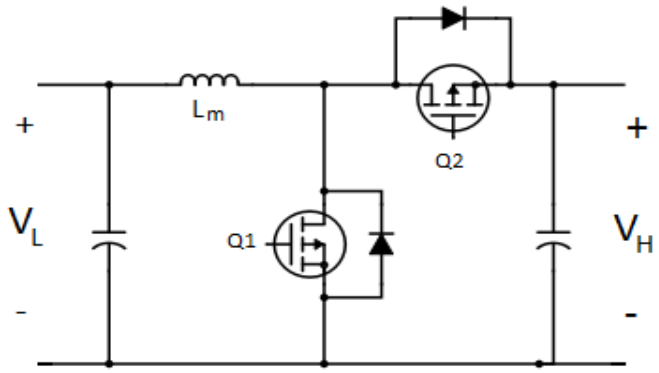

Figure 2-8 A bidirectional buck-boost converter

To get a fundamental understanding of how this topology works a switching analysis of the steady state will be made which describes how the buck and boost mode work. Some simplifications need to be made when explaining the dc steady state of the converter such as assuming ideal components, pure DC voltage in Vin and voltage out Vout and operation in continuous conduction mode (CCM) where the inductor current i_L flows continuously.

Boost mode is when a lower input voltage is converted into a higher output voltage, or when current flows from the lower voltage side to the higher voltage side. The switching analysis is done in two phases which describe the electrical characteristics of the circuit during switching. In Figure 2-9 an equivalent circuit can be seen for the first phase, when the switch S1 is conducting and switch S2 is blocking, during the interval

$$0 < t < DT_s \tag{2-7}$$

where D is the duty cycle and T_s is the switching period.

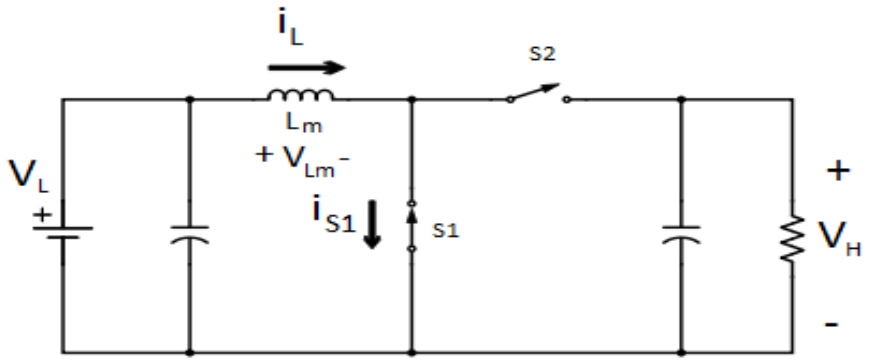

Figure 2-9 First phase of boost mode where s2 is open and s1 is closed

In this equivalent circuit the input voltage V_L is applied across the inductor making the input voltage equal the inductor voltage. The constant positive voltage across the inductor makes the inductor current increase linearly, thus increasing the inductor energy. This can be described using the formula

$$v_{Lm} = V_L = L_m \frac{di_{Lm}}{dt} \tag{2-8}$$

Since the inductor current increases linearly, the rate of change of the inductor current during the first phase can be described as

$$\frac{di_{Lm}}{dt} = \frac{\Delta i_{Lm}}{DT} = \frac{V_L}{L_m} \tag{2-9}$$

from which the change of inductor current during the first phase is

$$\Delta i_{Lm\,1} = \frac{V_L}{Lm} DT. \tag{2-10}$$

By switching S1 and S2 to their blocking and conducting states respectively the second phase is entered. An equivalent circuit for this phase can be seen in Figure 2-10. This occurs during the interval

$$DT_s < t < T_s. \tag{2-11}$$

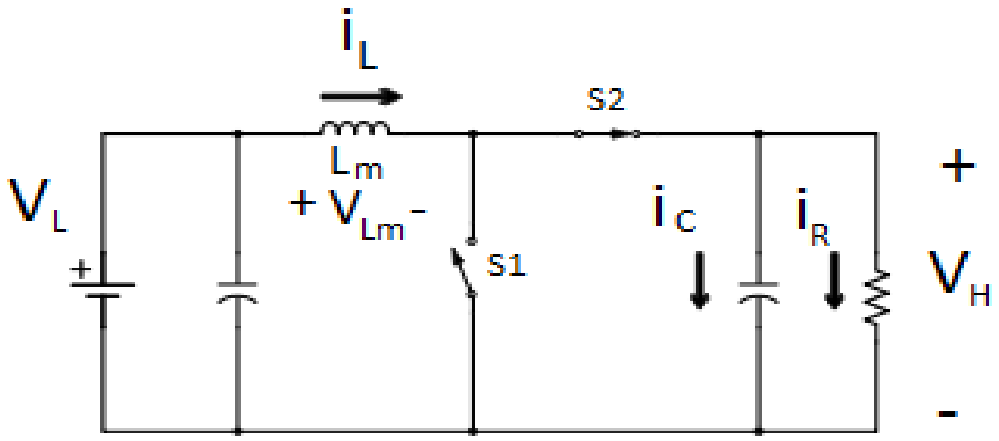

Figure 2-10 Second phase of boost mode where s2 is closed and s1 is open

During this phase the input voltage V_L is applied to one side of the inductor, while the output voltage V_H is applied to the other side. This constant negative voltage across means that the inductor voltage will decrease linearly and can be described using the formula

$$v_{Lm} = V_L - V_H = L_m \frac{di_{Lm}}{dt} \tag{2-12}$$

Since the inductor current decreases linearly, the rate of change of the inductor current during the second phase can be described as

$$\frac{di_{Lm}}{dt} = \frac{\Delta i_{Lm}}{(1-D)T} = \frac{V_L - V_H}{L_m} \tag{2-13}$$

from which the change of inductor current during the first phase is

$$\Delta i_{Lm\,2} = \frac{(V_L - V_H)}{Lm}(1-D)T. \tag{2-14}$$

Since steady state operation and continuous conduction mode is assumed the total change of current during one switching period equals zero. Using equation (2-10) and (2-14) leads to the formula

$$\Delta i_{Lm\,1} + \Delta i_{Lm\,2} = 0 \tag{2-15}$$

which can be expressed as

$$\frac{V_L}{Lm} \cdot D \cdot T + \frac{(V_L - V_H)}{Lm} \cdot (1-D) \cdot T = 0 \tag{2-16}$$

and simplified to

$$V_L.D + (V_L - V_H) \cdot (1-D) = 0 \tag{2-17}$$

which can be further simplified to reveal the voltage and duty cycle relation,

$$V_H = \frac{1}{1-D} \cdot V_L. \tag{2-18}$$

The other operation is the buck mode which can be explained in two phases. During the first phase the seen in Figure 2-11 the switch s2 is conducting and the switch s1 is off, the current will flow from high voltage V_H to the low voltage V_L through the inductor. The voltage over the inductor will then be

$$V_{Lm} = \frac{dI_L}{dT} L = V_H - V_L \tag{2-19}$$

where the positive current IL will lead to a linear increase due to the inductor. The total current change during this period can then be described by

$$\frac{\Delta I_{L(on)}}{\Delta T1} = \frac{V_H - V_L}{L_m} \tag{2-20}$$

where the time ΔT1 for the first phase is calculated as the product of the duty cycle D and the time T.

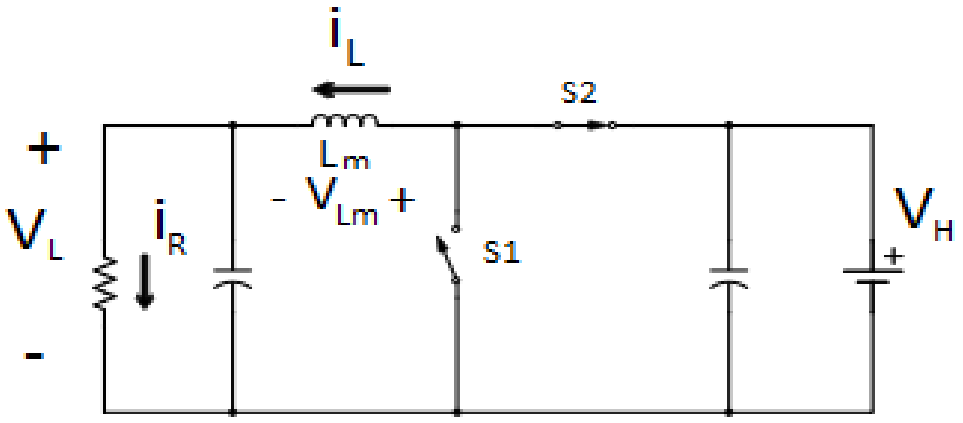

Figure 2-11 Phase one of buck mode where s1 is open and s2 is closed

During the next phase in Figure 2-12 the switch s2 is off and s1 is on. This is the same as the inductor being in parallel with V_L but with reversed polarization which means that

$$V_{Lm} = -V_L \tag{2-21}$$

and a negative voltage over the inductor is followed by a negative current derivative. This in turn means that the current change during this period can be calculated as

$$\frac{\Delta I_{L(off)}}{\Delta T2} = \frac{-V_L}{L_m} \tag{2-22}$$

where the time ΔT2 for the second phase will be decided by (1-D)T. By assuming the system to be under steady state the change of current must be equal to zero during one duty cycle, which means that

$$\Delta I_{L(on)} + \Delta I_{L(off)} = 0 \Rightarrow \frac{V_H - V_L}{L_m} \Delta T1 + \frac{-V_L}{L_m} \Delta T2 = 0. \tag{2-23}$$

Since ΔT1 is decided by DT and ΔT2 is decided by (1-D)T the formula concludes in the earlier discussed formula for buck converters being

$$\frac{V_H - V_L}{L_m} DT - \frac{-V_L}{L_m}(1-D)T = 0 \qquad \Rightarrow \qquad V_L = D \cdot V_H. \tag{2-24}$$

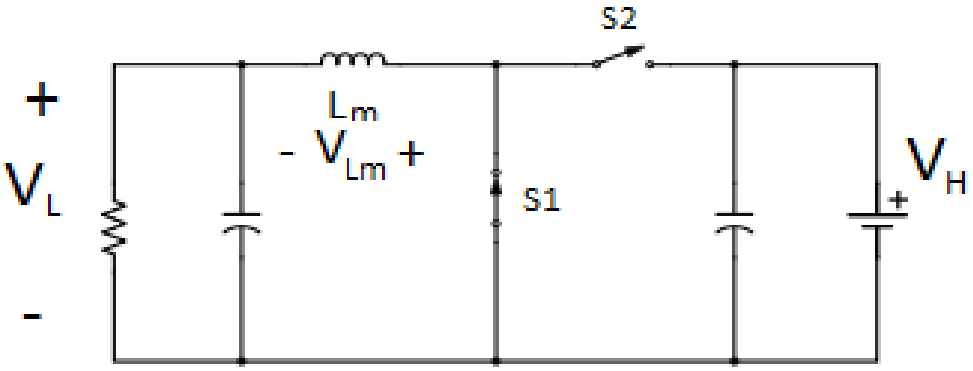

Figure 2-12 Phase two of buck mode where s1 is closed and s2 is open

2.2 MOSFET

In power electronics the switches in DC/DC converters are implemented using transistors. The metal oxide semiconductor field effect transistor (MOSFET) is a popular choice due to fast switching, voltage controlled switching and high input impedance [4]. The function of the component is to either conduct current during on-state and to block current during off-state. This is controlled by the gate voltage V_{GS}, where the MOSFET is in off-state if the gate source voltage V_{GS} is lower than the threshold voltage V_{TH} and in on-state when the gate source voltage is larger than V_{TH} [2].

2.2.1 Design Considerations

When designing a DC/DC converter it is important to understand the negative properties of the MOSFET. According to [4] one crucial parameter is the dV/dT capability when operating at high frequency since high frequency means small dT. What might happen is that the MOSFET could accidentally turn on if the gate resistance is too large and there is a large dV/dT since

$$v_{GS} = i_{GD} \cdot R_G = R_G \cdot C_{GD} \cdot \left(\frac{dV_{DS}}{dT}\right) \tag{2-25}$$

and V_{GS} could get larger than V_{TH}. The following equation can be used to calculate the maximum dV/dT

$$\left(\frac{dV}{dT}\right)_{max} = \frac{V_{TH}}{R_G \cdot C_{GD}} \tag{2-26}$$

which shows that R_G need to be sufficiently small at high frequencies [4]. The other negative property is the parasitic BJT inside the MOSFET which according to [5] is more likely to occur in bridge circuits. The issue is similar to the last one that MOSFET could accidentally turn on during fast switching. Therefore, the solution is also similar, to slow down the switching speed either by using a larger gate resistance or other methods such as negative

bias. This is why the value for the external gate resistance needs to be selected carefully since it should neither be too big or too small.

When designing a circuit containing MOSFETs on a PCB for high frequency applications it is important to think about the stray inductances. Parasitic inductance will appear both from the MOSFET packaging but also in the capacitors and from the PCB traces. What can appear is that the MOSFET is overstressed due to high V_{DS} if the stray inductances are too large since

$$V_{DS(turn-off)} = V_D + L\frac{dI}{dT} \qquad (2\text{-}27)$$

where a V_{DS} overvoltage can damage the MOSFET.

2.2.2 Power Losses

The power losses in the MOSFET are correlated to switching frequency as well as the average dissipation during on-state. The equation for switching losses is the following

$$P_s = 0.5V_d\, I_o\, f_s\, (t_{c\,(on)} + t_{c\,(off)}) = 0.5V_d\, I_o\, f_s\, (t_{ir} + t_{vf} + t_{if} + t_{vr}) \qquad (2\text{-}28)$$

where I_o is the current through the MOSFET, f_s is the operating frequency and $t_{c(on)}$, $t_{c(off)}$ are derived from the MOSFET electrical characteristics. The time $t_{c(on)}$ is the time it takes for the current to rise and the voltage to drop when turning on the switch and $t_{c(off)}$ is the opposite, the time it takes for the current to drop and the voltage to rise during turn off. In order to calculate the power losses during turn on, Figure 2-13 is used to represent the MOSFET characteristics. The turn on period is divided into three time intervals which are used when calculating switching losses. t1 is defined as the time it takes for the gate to source voltage V_{GS} to charge the MOSFET capacitances and reach the threshold voltage V_{TH}. The drain-source current Ids will rise until it reaches the maximum load current at the end of t2. The current rise time t_{ir} is therefore defined as t2-t1. After t2 the voltage V_{DS} will start to decline and V_{GS} remains in what is called the plateau voltage V_{GP} and charges the Miller capacitance C_{GD} with the current i_G, the time for the voltage to fall t_{vf} is therefore given by the time t3 shown in Figure 2-13 [4].

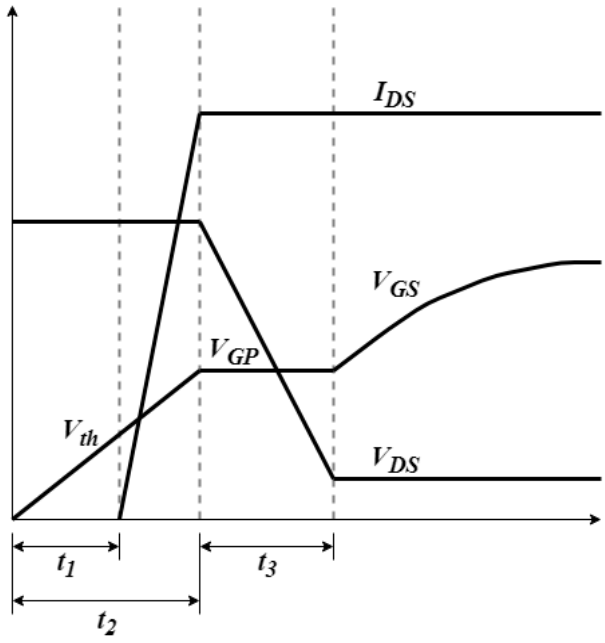

Figure 2-13 MOSFET turn on characteristics

The turn off period is shown in Figure 2-14 and is also divided into three time intervals that are used for the power losses calculations. The time period t4 is the delay time it takes to discharge the gate voltage V_{GS} to the plateau voltage V_{GP} which is followed by the voltage V_{DS} beginning to rise. At the end of t4 the miller plateau is reached, and the current and gate-source voltage is constant while the voltage is increasing. t5 is the time it takes for the voltage to reach the supply voltage while t6 is the time it takes for current and gate source voltage to decline to zero [4].

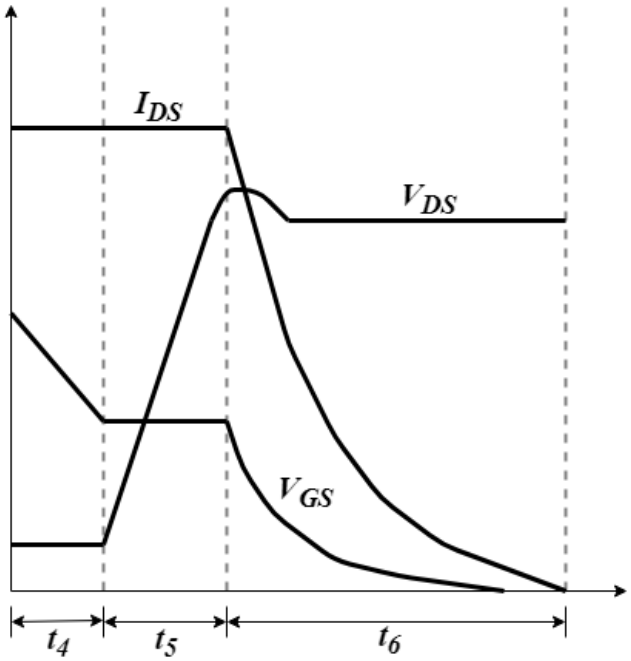

Figure 2-14 MOSFET turn off characteristics

Following the instructions from [6] the voltage rise and fall times can be calculated using the following equations

$$t_{VR} = t_5 = \frac{Q_{gd} \cdot R_{goff}}{V_{GP}} \tag{2-29}$$

and

$$t_{VF} = t_3 = \frac{Q_{gd} \cdot (R_g + R_{g-on})}{V_{GS} - V_{GP}} \tag{2-30}$$

where R_g is the MOSFET gate resistance, Q_{qd} is the gate to drain charge and R_{gon}, R_{goff} is the external resistances when the MOSFET is turning on or off. According to [6] the accuracy of the calculation for current rise and fall time can be increased if the source package inductance L_S is taken into consideration to include the effects of current transients. The equations that can be used to calculate the current rise and fall time is then

$$t_{IR} = t_2 - t_1 = (R_g + R_{g-on}) \cdot C_{iss} \cdot ln\left(\frac{(V_{GS} - V_{TH}) + \frac{(V_{GS} - V_{TH}) g_{fs} L}{(R_g + R_{g-on}) C_{iss}}}{V_{GS} - V_{GP}}\right) \tag{2-31}$$

and

$$t_{IF} = t_6 = (R_g + R_{g-off}) \cdot C_{iss} \cdot ln\left(\frac{V_{GP}\left(1 + \frac{g_{fs} L}{(R_g + R_{g-off}) C_{iss}}\right.}{V_{TH}}\right) \tag{2-32}$$

where C_{iss} is the input capacitance consisting of C_{GS} and C_{GD}, g_{fs} is the transconductance and V_{TH} is the threshold voltage. This concludes the times needed for calculation the switching losses for the MOSFET. The power losses from the average dissipation during on-state for a DC/DC converter is calculated with the equation

$$P_{on} = V_{on}\, I_o\, \frac{t_{on}}{Ts} = r_{on} I_{on}^2 \frac{t_{on}}{Ts} \tag{2-33}$$

where the time $\frac{t_{on}}{Ts}$is the same as the duty cycle D and r_{on},I_{on} is the drain-source resistance and current,$R_{DS}$and I_{DS} during on-state [5].

2.3 Inductor

When designing a DC/DC converter it is important to consider the design of an inductor as well since inductors are not widely commercially available. This is because they are most often designed for specific applications.

2.3.1 Design of Inductor

In suggested design calculations from Texas Instruments [7] the following equations can be used to select appropriate inductor with an inductance L,

$$L > \frac{Vout \cdot (Vinmax - Vout)}{K_{ind} \cdot Fsw \cdot Vinmax \cdot Iout} \tag{2-34}$$

for a buck mode converter and

$$L > \frac{Vinmin^2 \cdot (Vout - Vinmin)}{K_{ind} \cdot Fsw \cdot Iout \cdot Vout^2} \tag{2-35}$$

for boost mode, where V_{inmax} is the maximum input voltage, V_{out} is the output voltage, I_{out} is the rated output current, F_{sw} is the switching frequency and K_{ind} is the maximum current ripple. The largest value of these inductances is selected.

When selecting a core there are two major classes, ferrites and alloys. Due to small eddy current losses ferrite cores are a good choice at frequencies higher than 10 kHz but has lower saturation flux density while alloy cores have higher saturation flux density but suffers from higher eddy current losses at higher frequencies. The relationship between flux density B, flux Φ, core cross-section area Ae can be seen as

$$B = \frac{\Phi}{A_e} = \frac{N \cdot I}{A_e \cdot (R_{gap} + R_{core})} \tag{2-36}$$

where the reluctance R_{gap} will get bigger with a larger air gap. This results in a limitation to the magnetic flux being

$$\Phi = \frac{B}{A_e} \tag{2-37}$$

which limits the amount of turns N by a maximum

$$N = \frac{\Phi \cdot R_{tot}}{I} \tag{2-38}$$

and with the decided amount of turns, the inductor value of L can be calculated by

$$L = \frac{N^2}{R_{tot}} \text{[5].} \tag{2-39}$$

2.3.2 Power Losses

The inductor power losses are divided into two parts, winding losses and hysteresis losses of the core. At higher frequencies the skin effect needs to be considered, where eddy currents flowing in the opposite way as the conductor current are generated by the magnetic fields of the conductor current. These eddy currents flow in the middle of the conductor which in turn forces the conductor current to flow near the edges of the conductor approximately one skin depth deep. This decreases the cross-sectional area the current can flow through which in turn increases resistance and power dissipation. A graph showing the skin depth of different materials at multiple frequencies can be seen in Figure 2-15 [5].

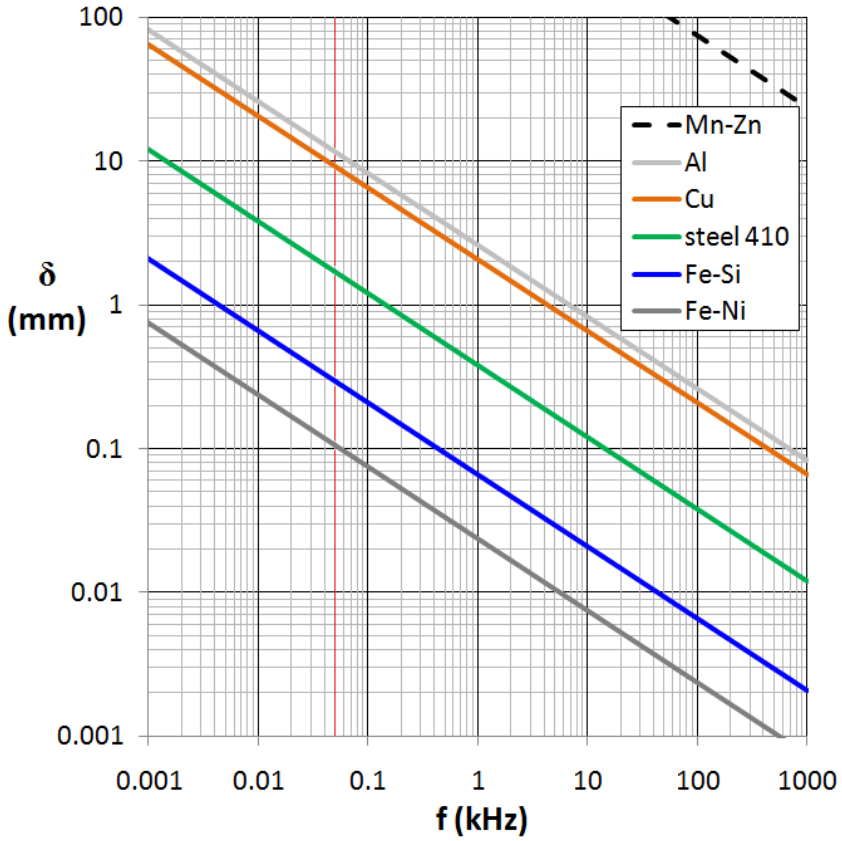

Figure 2-15 The skin depth of different materials at different frequencies by Zureks [CC0], from Wikimedia Commons

By using Litz wire with a strand diameter of less than or equal to two times the skin depth the skin effect can be neglected. In the common case of a copper conductor the winding losses caused by the DC resistance in the copper remain. The power losses are calculated by

$$P = \rho \cdot k_{cu} \cdot J_{rms}^2 \cdot V_w \tag{2-40}$$

where ρ is the resistivity of copper, k_{cu} is called the fill factor given by, J_{rms} is the current density and V_w is the total winding volume given by core dimensions [5]. To minimize these power losses the design of the conductor must be taken into consideration. If a Litz wire with multiple strands is used it is possible control the total cross section area of the copper wire A_{cu} since

$$A_{cu} = A_z \cdot z \tag{2-41}$$

where A_z is the strand cross section area and z is the amounts of Litz strands. By changing the area A_{cu} it is possible to decrease the current density J_{rms} is given as

$$J_{rms} = \frac{I_{RMS}}{A_{CU}} \tag{2-42}$$

but at the same time increasing the fill factor k_{cu} since

$$k_{cu} = \frac{N \cdot A_{cu}}{A_w} \tag{2-43}$$

which gives the designer the possibility to decrease the power losses. It is also important to have a sufficiently large A_{cu} for high current applications [5].

The hysteresis losses are based on the magnetic characteristics of the core material which theory will not be provided. The value P_v can usually be found in the datasheet for the core material where P_v is based on the frequency f of the system and the AC field flux density $\hat{B}$. The hysteresis power losses are then calculated by

$$P_{core} = V_e \cdot P_v \tag{2-44}$$

where V_e is the total magnetic core volume given in mm^3.

2.4 Thermal Considerations

One of the most important parameters for a power electronics system is the efficiency. The system should optimally be designed to have as little power losses as possible. The efficiency is in general given by

$$\eta = \frac{P_{OUT}}{P_{IN}} \tag{2-45}$$

where η is usually given in percent. The converter is very dependent on power losses in the system since it will affect the layout and the need for cooling. The two big contributors of power losses are usually the transistors and the inductors due to conduction and switching losses.

Thermal considerations are necessary since power electronic components suffer detrimental characteristics if internal temperatures rise. For example, increasing the junction temperature of a MOSFET increases the on-state resistance significantly, which in turn leads to higher power dissipation in these power semiconductors [5].

When considering the thermal properties of a system, the worst-case junction temperature needs to be specified. In order to have a design intended for high reliability, having a worst-

case junction temperature of 20 ℃ to 40 ℃ below 125 ℃ is recommended. It should be not be noted that some components can operate above 200 ℃, however the performance and lifetime may be poor. The thermal layout is something to be considered at an early stage of system design since size, weight and temperature of surrounding components of the system are affected by the chosen cooling solution [5]. In an energy dense system, using surface-mount devices (SMD) close together to minimize stray inductance, the heatsink can be mounted on the opposite side of the components on the PCB. The heatsink is connected to the power components by vias through the pcb that will conduct the power dissipated while providing some insulation to the other components on the PCB.

The location where the system is placed is also of importance, since heatsinks can be very large compared to PCBs. The fins of the heatsinks needs to be positioned vertically in the case where no fan is present, for natural convection of the air to function optimally. The ambient temperature is also a design input that depends on the location of the system [5].

Most of the power dissipation in power transistors that needs to be removed is done by conduction to a heat sink that in turn uses convection and radiation to transfer heat to the air. The conduction is often through several different layers of various materials with different thermal characteristics. These layers have a specific thermal resistance, which determines its ability to transfer power from one temperature potential to another. Such a case with multiple layers can be seen in Figure 2-16a. The relation between the power, temperature and thermal resistance can be described with

$$P = \frac{\Delta T}{R} \qquad (2\text{-}46)$$

and is analogous to the electrical relation between voltage, power and resistance respectively. As such an equivalent circuit for the heat flow can be modeled after an electrical circuit as can be seen in Figure 2-16 b. The analog holds true in the case of parallel paths for the power, where the same relation as parallel resistors in an electrical circuit can be used to model the thermal circuit [5].

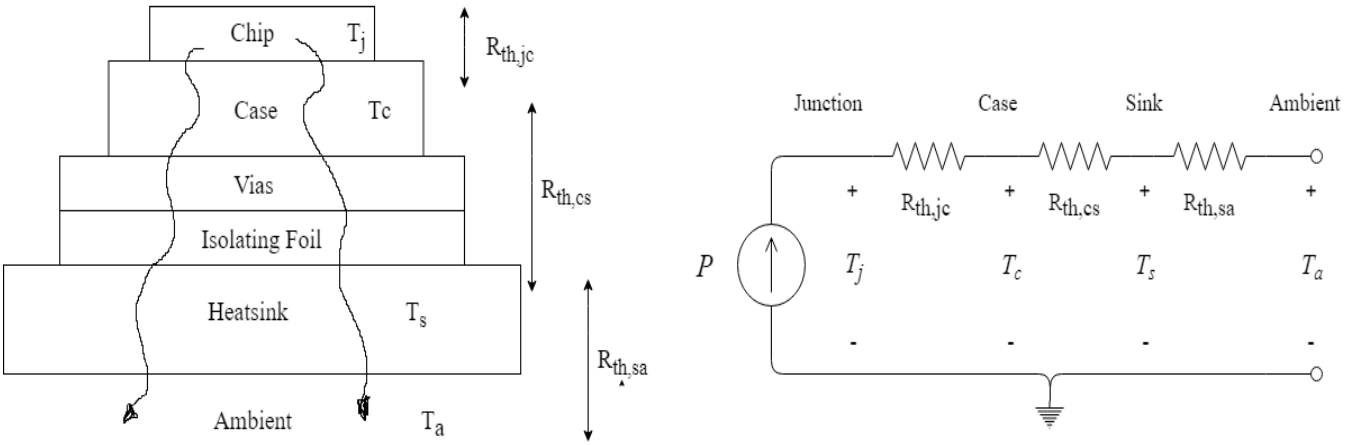

Figure 2-16 Thermal circuit model

2.5 PV cells

The solar cell is an electric component with the ability to produce energy from sunlight. The solar cell is more commonly called a photovoltaic cell (PV cell), where the term photovoltaic originates from the conversion of light into electricity. The most common model for the PV cell is the simplified model shown in Figure 2-17. This model does not take losses into consideration and only represents the PV cell with a current source and a diode in parallel but is sufficient for this study since the PV modules are purchased and not analyzed in detail [8].

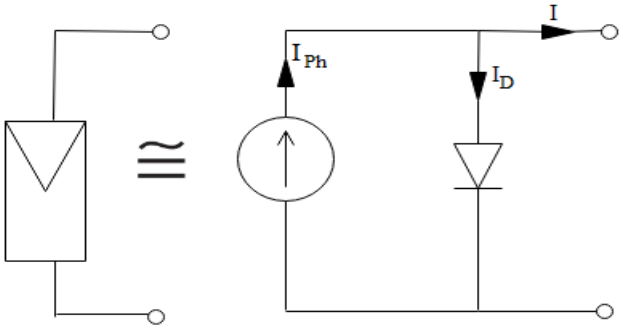

Figure 2-17 Simplified model of the PV cell

2.6 Batteries

Every battery has a capacity C often expressed in Ampere hours, Ah, which determines the amount of charge that can be stored in a battery. The capacity is however not constant but varies depending on the discharge current. This means that if the drawn current is larger, not as much charge can be extracted from the battery. That is why a nominal current is needed together with a nominal capacity in order to ascertain the relevant properties. For example, C_{10} is the capacity when the current $I_{10}$is drawn, which in turn is the current that completely discharges the battery in 10 hours. Temperature also has an effect on the capacity, where lower temperature correlates with lower capacity [8].

Necessary parameters for the battery is the State of Charge (SoC) and the Depth of Discharge (DoD). The SoC describes the state of the battery capacity in percentage meaning that for example 100% SoC is a fully charged battery and DoD is the complement of SoC, which would be 0% DoD in this case. The units are usually used to describe the current state or the lifetime of the battery. To calculate the SoC the current can be integrated over time. This method is called coulomb counting. The downside to this calculation is that it is impossible to know the SoC at startup, the battery voltage must first reach the maximum voltage to set the SoC to 100% after which it can start calculating the SoC [9].

Batteries modeled as a voltage source have a voltage tied to them. The voltage of a battery depends on how many voltaic cells are connected in series and their individual voltage which varies depending on which type of cells are used. The voltage varies depending on the SoC, where the voltage goes down with decreasing SoC.

To calculate the energy, W in Wh, that is available in a battery the formula,

$$W = C_{nom} \cdot DoD_{max} \cdot U_{nom} \tag{2-47}$$

can be used where W is the energy in Wh, C_{nom} is the nominal charge, DoD_{max} is the maximum allowed depth of discharge and U_{nom} is the nominal voltage [8].

2.7 Battery Management System

For standalone systems it is very important to keep the batteries at good health, both for safety and sustainability. With a battery management system (BMS) it is possible to keep track of the batteries to avoid overcharging and over discharging to increase the lifespan. It is important to avoid frequent deep discharges of the battery since this will reduce the capacity of the battery. Every battery has their own description on how to increase the lifespan of the battery, but a rule of thumb is that the state of charge should never be less than 30% in order to have a good lifespan. The BMS keeps track of the voltage, current and temperature to make sure that the state of the battery is controlled while balancing charge between the cells to keep cell voltage the same to make sure that the battery is not damaged [8]. This can be done with the use of a microcontroller which can regulate the current and voltage of batteries depending on several variables such as the SoC and ambient temperature. For example, the charging of a battery by controlling the duty cycle of the PWM of a converter [10]. For software purposes to ensure good battery health it is sometimes common to change the SoC to where 0% SoC is the maximum allowed DoD and 100% SoC is the limit stated by maximum cell voltage. An example of this can be seen in Figure 2-18, where a new SoC has been applied, represented by the green area.

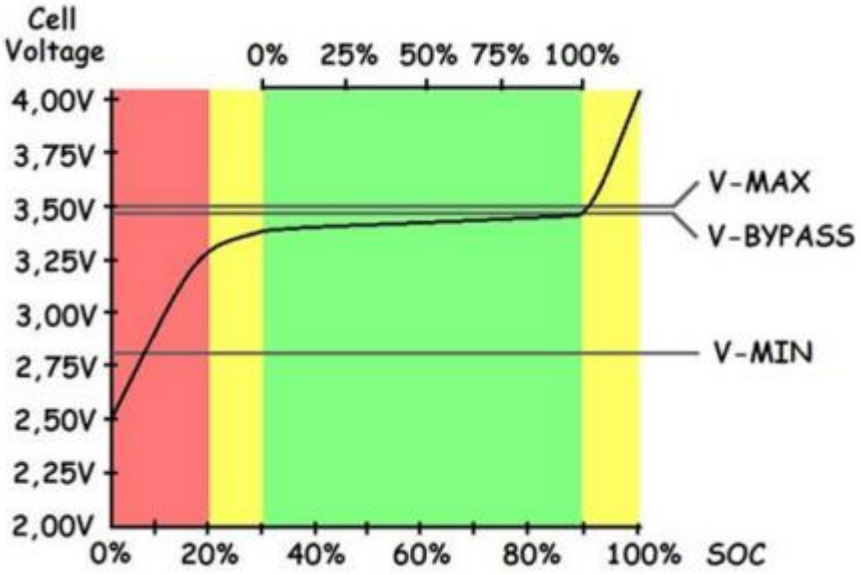

Figure 2-18 State of charge in a battery, Copyright © 2018 EV Power, Reprinted by permission of EV Power.

In order to not overcharge or overdischarge batteries a charge controller can be used to protect the batteries. By knowing the state of charge and voltage of a battery, a charge controller can regulate when to disconnect the battery to protect from overdischarge and how to properly charge a battery. A type of charge controller for a lead-acid battery is programmed to first charge with constant current into the battery. When the end-of-charge voltage is reached it changes to charge with a constant end-of-charge voltage for a time, about 1-3 hours. After that the battery is trickle charged by keeping the charging voltage constant at the nominal voltage of the battery, where the battery will draw a small maintenance current. It should be noted that each battery is different and should be charged and discharged according to the manufacturers specifications [10].

2.8 Driver circuit

In order to switch a power transistor with a microcontroller, a driver circuit is needed. The purpose of the driver is to provide a large gate voltage and current to improve the power transistor characteristics while also providing electrical isolation between the digital logic circuit and the power transistor. It is usually an integrated circuit (IC) with different features to improve the switching properties and can be implemented with different solutions [5].

For half bridge converter topologies, where the upper transistor will have a so called floating ground, a bootstrap circuit is needed in addition to the driver circuit. Floating ground means that the gate source voltage V_{GS} is referenced to ground but the source for the upper transistor will swing between ground and a high voltage when the lower power transistor is switching. The bootstrap circuit contains of a diode, a resistor and a capacitor. The diode will charge the bootstrap capacitor when the lower power transistor is on and it will discharge when the upper transistor turns on [11].

3 Method

In order to answer our questions and problems the method will be divided into different steps. The first step is the specification of the system followed by simulating and designing the hardware. When that is done the last step is to test and evaluate the software in a test circuit. The method that is used in this project is based on an engineering design process which is a common approach to problem solving and design evaluation [12]. The method was chosen because of its simple yet effective iterative approach to solve technical problems. An example of this method can be seen in Figure 3-1. In our case the method can be divided more precisely into three steps which are pre-study, simulation and design and finally test and evaluation. This is an effective way to get an overview of the process for creating the bidirectional DC/DC converter and the battery management software.

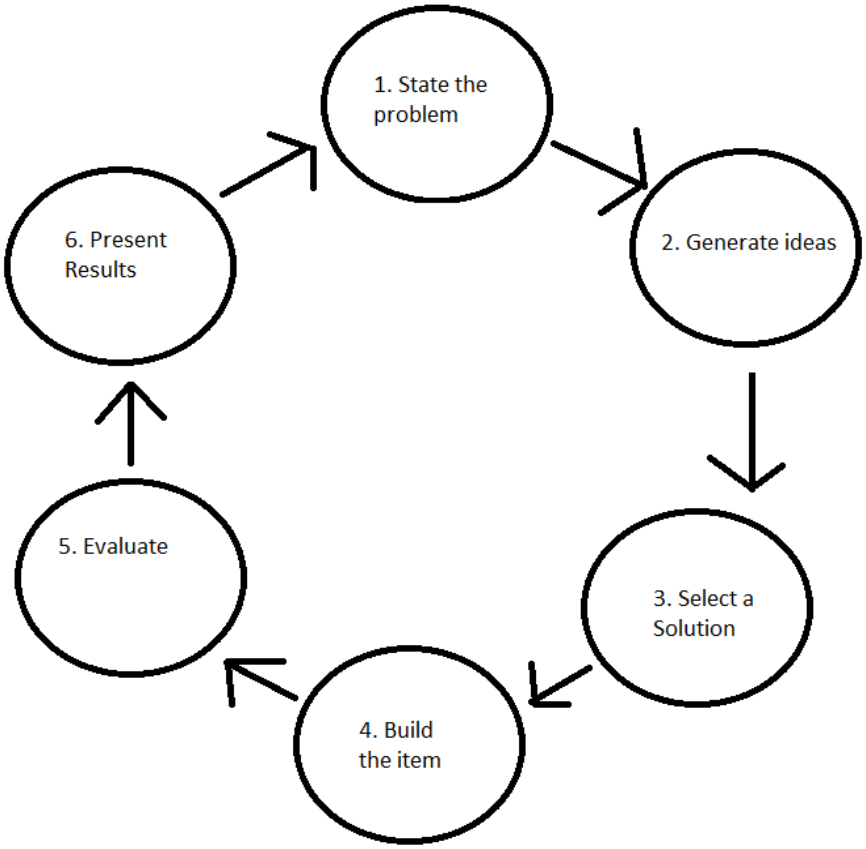

Figure 3-1 The steps of the engineering design process

3.1 Pre-study

To get a good starting point for the design of DC/DC converter a pre-study was made. This includes finding relating articles and respectable sources for the surrounding theory, choosing a topology, describing the entire system, power flow analysis and creating a specification for the design.

3.1.1 System Overview

As a continuation of the background, an explanation of the proposed overall system is presented, seen in Figure 3-2. The overall system will be composed of two batteries, one 12 V battery and one 48 V battery. The two batteries are interconnected with a bidirectional DC/DC converter that allows energy to be transferred between the two batteries in both directions. There are two PV panels, each with their own converters provided with maximum power point tracking (MPPT). These are connected in parallel and will output a current depending on the solar irradiation that will charge the 12 V battery. The 12 V battery is also connected to a load which represents the different devices that require 12 V to function, such as GPS, phone charger and lamps. The 48 V battery is connected to a bidirectional DC/AC converter that in turn is connected to a BLDC-motor. The motor can generate thrust by consuming energy and, while sailing, it can work as a generator and generate energy regeneratively by breaking.

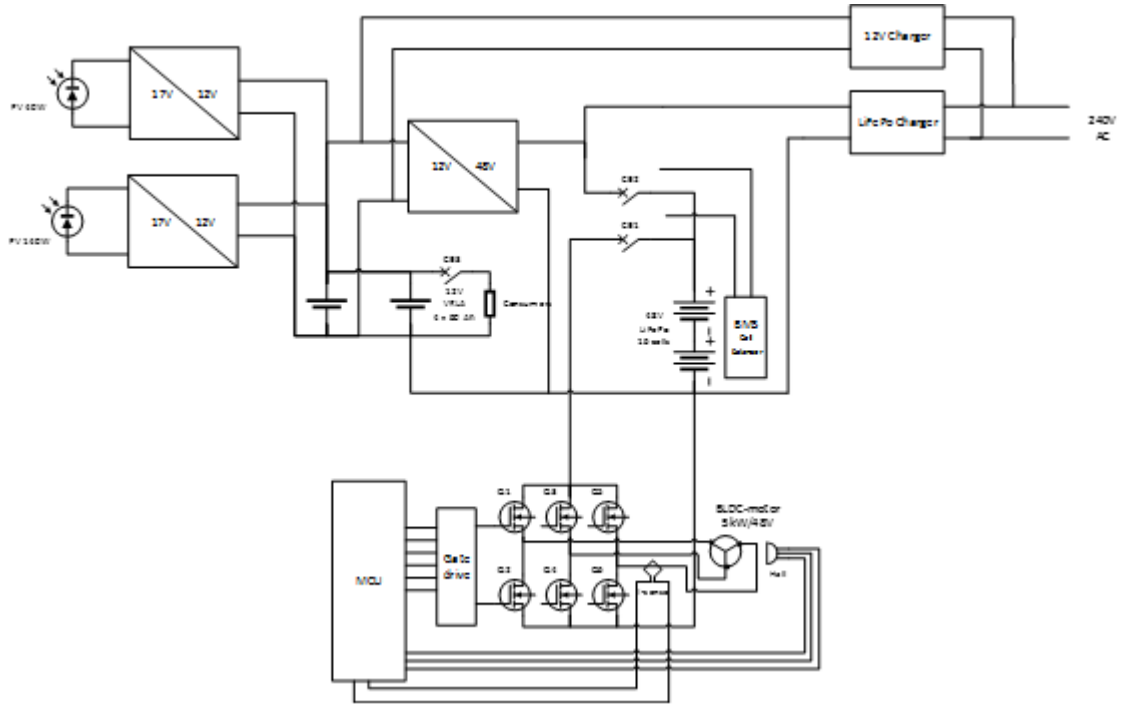

Figure 3-2 System overview

The 48 V battery is provided with its own BMS system that keeps the battery cells in good condition and can provide various information such as temperature that will be transferred to the Arduino. The Arduino will be in charge of measuring the voltage and current of both batteries to calculate SoC which will be used as an indicator when energy should be transferred. This will work as the BMS of highest hierarchy that controls the system.

3.1.2 Energy Calculations

In order to get a good overview of the energy transfer capabilities required of the converter a test case is proposed where approximations on the energy generated, energy consumed as well as energy transferred are made. The test case is made to emulate a field test with large margins of errors.

3.1.2.1 Test Case

Table 3-1 shows a simplified version of the energy available and what output and input energy is expected in the system using the values given for batteries and PV panels in the appendix (8).

Table 3-1 Values from test case

Battery	12 V	48 V	Total
Total capacity [Wh]	2765	2304	5069
Output energy [Wh/day]	555	1333	1888
Input energy [Wh/day]	552	300	852

The total capacity of the batteries is taken from their respective specifications and the available energy for the respective batteries can be calculated using (2-47)

$$W_{12} = C_{nom,12} \cdot DoD_{max,12} \cdot U_{12,nom} = 384 \cdot 0.6 \cdot 12 \approx 2765 \text{ Wh} \quad (3\text{-}1)$$

$$W_{48} = C_{nom,48} \cdot DoD_{max,48} \cdot U_{48,nom} = 60 \cdot 0.75 \cdot 48 \approx 2304 \text{ Wh} \quad (3\text{-}2)$$

It should be noted that this energy is what is available without deep discharging. More energy can be extracted at risk of decreasing the expected lifetime of the battery. The output energy of the 12 V battery is approximated using normal values for the different electrical consumers on the boat such as a refrigerator, GPS and lamps. The output energy of the 48 V battery is calculated from one hour of driving at 5 knots with a battery to motor efficiency of 75%. The input energy to the 12 V battery is approximated by assuming the PV panels get 3 hours of 1000W/m^3 solar irradiance per day. The input to the 48 V battery which is from when the generator mode is on during sailing, is approximated to be 150 W and turned on 2 hours a day.

As can be seen in Table 3-1, without energy transfer the 48 V battery will run out in about 2 days and with lossless energy transfer both batteries will run out in about 5 days in this test case.

3.1.2.2 Energy Transfer

Since losses are prevalent in a converter it is a good idea to try to limit the amount of power that needs to be converted. Optimally the converter does not need to be used and only the power generated from the generator and solar panels is consumed by their own respective circuits. But in most cases including our test case the energy consumed exceeds the generated amount, a strategy for energy transfer needs to be made to minimize losses. Designing an optimal strategy for efficiency is however not possible since, unlike our test case, the energy consumed and generated is unpredictable and varies. In the scope of this project a simpler strategy will be proposed due to limitations. This strategy aims to equalize the charge of the batteries so that the batteries of each circuit can store the power that is generated in each

respective circuit. It will accomplish this by transferring energy quickly if the difference in each batteries state of charge is large and slowly if the difference is small. It will stop transferring when the difference in SoC of the batteries are similar. An initial strategy for these transferring limits can be seen in Figure 3-3.

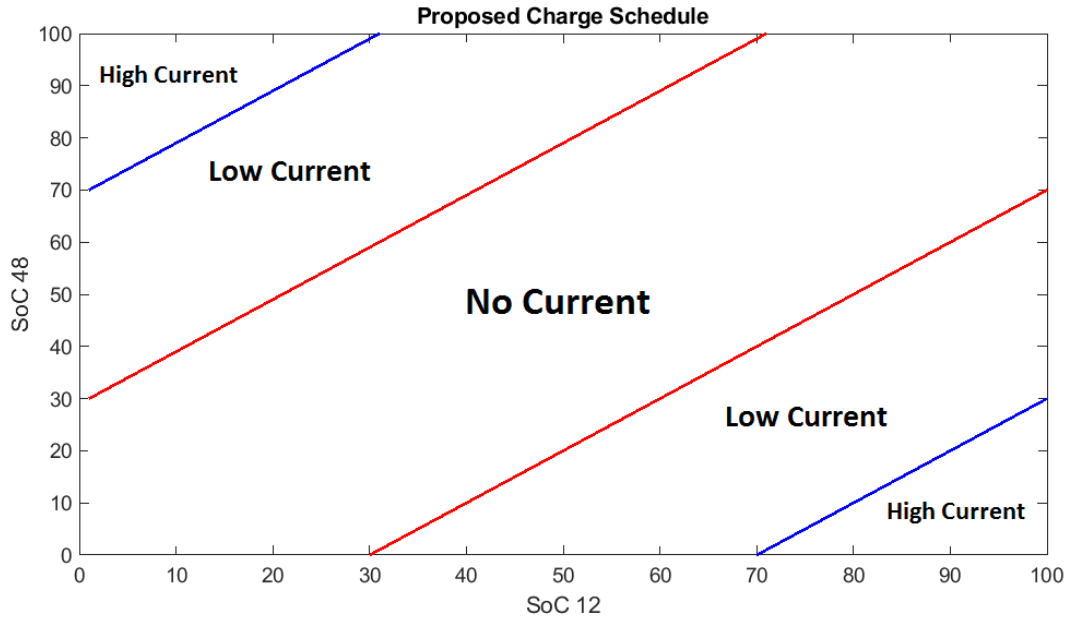

Figure 3-3 Proposed charge schedule where the SoC for the 48 V battery is on the Y-axis and the SoC for the 12 V battery is on the X-axis

3.1.3 Comparison of Bidirectional Buck-Boost

The two batteries in the system will work together using a bidirectional buck-boost converter. This opens the possibility to charge and discharge both batteries which is needed to optimize the power flow. To decide the design of the dc/dc converter a comparison between different topologies and solutions are needed.

3.1.3.1 Four-Switch Noninverting Buck-Boost Converter

The four switch non-inverting buck-boost converter is a common design for bidirectional DC/DC converters. As the name implies, the converter consists of four switches and the topology has some benefits and drawbacks. According to Ioinovici, A. [13] the potential range of input voltages for the design is beneficial for battery applications. The topology allows the boost and buck operations to have stable transition between modes. Yu. et. al. [14] shows how Zero Voltage Switching (ZVS) can be used to achieve higher efficiency. The experiment showed that the losses in the switches and passive components could be reduced by the use of a diode and capacitor in parallel with the MOSFET switches. The experiment with their 3 kW prototype showed that an efficiency between 97.79 % and 99.60 % was achieved. Another study made by Ouchi. et. al. [15] used this topology for an energy system containing PV modules with a possibility to charge and discharge up to 20 kW. They achieved an efficiency of 97.8% with their 5 kW prototype and concluded that the topology works well for an energy system.

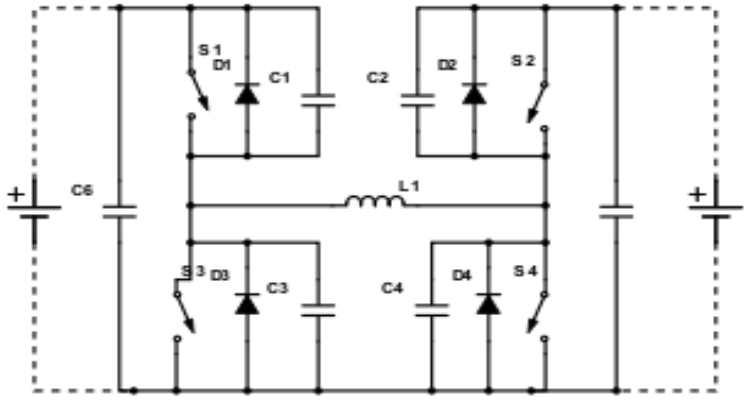

Figure 3-4 Four-Switch Noninverting Buck-Boost Converter circuit

3.1.3.2 Two-Switch Buck-Boost Converter

The two-switch bidirectional buck-boost converter is a simpler design when it comes to buck-boost converters, using two switches and a single inductor and can be seen in Figure 3-5. Xu. et. al. [16] shows how this topology can work using non-synchronous switching where it works as a buck converter if Q2 is set to be blocking while Q1 is controlled according to how a generic buck converter is regulated. For boost mode, Q1 is set to be conducting while Q2 is switched according to how a boost converter is regulated. By implementing this bidirectional buck-boost converter in a battery charging circuit an efficiency of 96 % was reached. Chao. et. al. [3] showed how this topology can be implemented in a PV system where the charging and discharging of a battery required to be controlled using an energy management strategy. This study used synchronous switching, stating increased conversion efficiency.

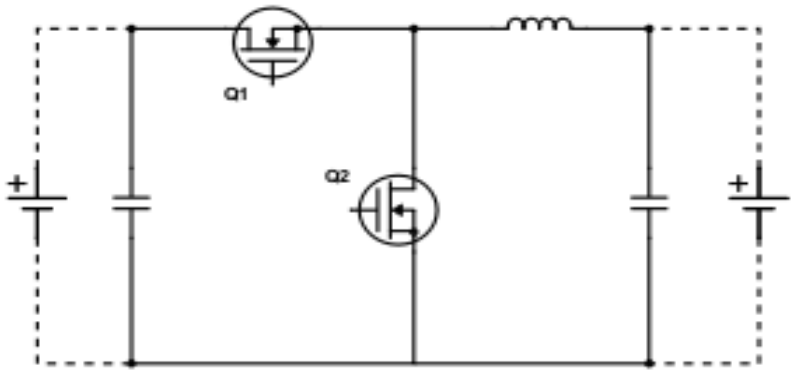

Figure 3-5 Two-switch bidirectional buck-boost converter

3.1.4 Choice of Topology and Specification

After comparing different topologies, the two-switch bidirectional synchronous buck-boost converter was chosen for its less complex design and implementation. This was important due to the time limitation of the project. In order to minimize the capacitors and inductor while still having acceptable switching losses a switching frequency of 50 kHz was chosen. In Table 3-2 the chosen specification can be seen. The motivation behind the RMS output current of 40

A was due to the possibility of charging the 12 V battery with at least 10% of the capacity being 38.4 A. The current ripple for charging the battery be specified to maximum 15% since a larger current ripple may affect the battery lifespan.

Table 3-2 Specification for the system

Specification	Input voltage	48 V	Output voltage	12 V
	RMS input current	10 A	RMS output current	40 A
	Rated power	480 W	Output current ripple	15%
	Switching frequency PWM	50 kHz	$I_L$max	46 A
	Max MOSFET voltage peak VDS	120 V		

3.2 Simulation

The simulations of the system were divided into two parts, overall simulation of the topology in MATLAB Simulink. More detailed simulation of components and driver stage in MultiSIM. The reason for this is that Simulink have more detailed models of batteries while MultiSIM has better possibilities of simulating non-ideal components. Simulink also has support for Arduino which is very useful when developing the software for later.

3.2.1 Simulink Simulation

In Figure 3-6 the topology simulation in Simulink can be seen. Measurements of voltages and currents were made to make sure that the specification was fulfilled. The duty cycle was simulated using a DC PWM block with a constant value that could be changed during simulation. To simulate synchronous switching a NOT-gate was used to invert the duty cycle for the boost MOSFET.

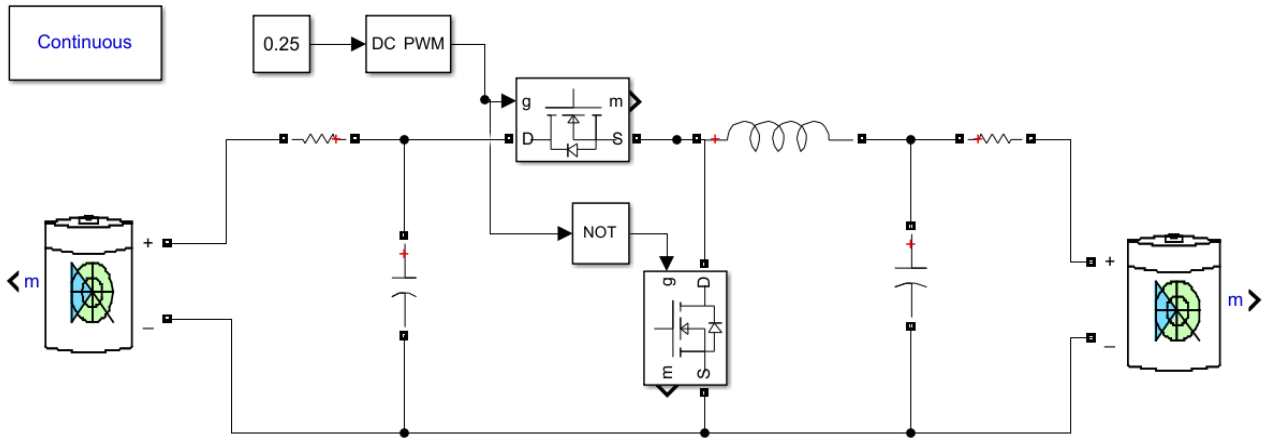

Figure 3-6 Topology simulated in MATLAB Simulink

3.2.2 Multisim Simulation

To ensure the specification for the chosen MOSFET IPB044N15N5 simulations of the switching characteristics were made in MultiSIM. To simulate the potential overvoltage from parasitic inductances discussed in 2.2.1 that occurs when the upper MOSFET switches, the circuit in Figure 3-7 was used. Different values for components were used to make sure the specification was met. The constant current source represents the current in the inductor. To represent the DC bus connected to the 48 V battery, the capacitors of 75 µF and 400 µF with their parasitic inductances of 1 nH and 6 nH are used. This method was used to decide the values of the external resistances R_{gon} and R_{goff}.

To provide more exact simulations the models for the driver circuit and the MOSFET that were used are provided by the manufacturers. As these models are made by the manufacturers they contain more trustworthy parameters and characteristics to emulate the component.

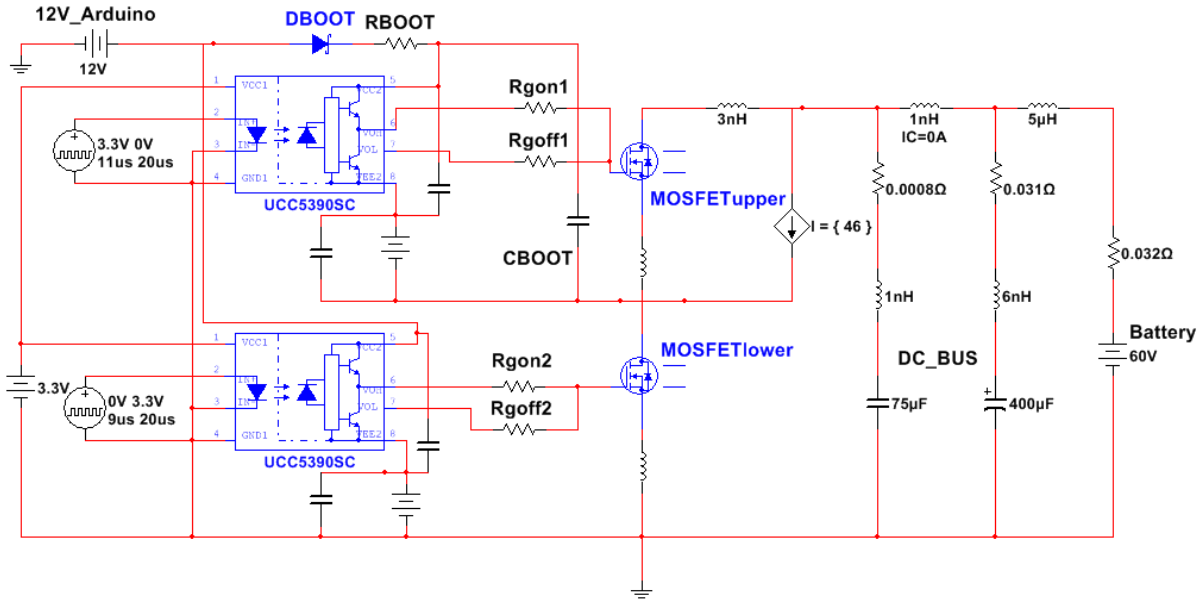

Figure 3-7 MOSFET simulation test circuit without component values in MultiSIM

3.3 Components and Design

All components need to be chosen so that the specifications are met. A certain safety margin is added to ensure that components do not break even when exceeding specification if for example an error in the system occur.

3.3.1 MOSFET

When selecting a power MOSFET for the DC/DC the most crucial parameters are the high voltage and current. Due to availability for early testing and being sufficient for the application the MOSFET IPB044N15N5 from Infineon was selected [17]. With the parameters of 150 V V_{DS} and 174 A I_D it is probably overkill for this application and was selected because of familiarity and coincidences.

3.3.2 Driver Circuit

To be able to turn the MOSFETs at a switch frequency of 50 kHz a driver circuit is needed. The chosen driver circuit is the integrated circuit UCC5390SC. The IC is a suitable candidate due to the high output voltage to minimize losses in the MOSFET but also the high sink and

source current which is important for fast switching. The functional block diagram for the driver can be seen in the datasheet on page 28, figure 52 [18]. How this topology works is that when the PWM signal is high from the microcontroller, the driver circuit switches the internal parallel transistors to connect the voltage V_{CC2} to the gate for fast turn on. When the PWM is low the driver circuit switches the lower transistor to connect the gate to ground. The integrated circuit provides a split output which allows the use of separate external resistances to control the rise and fall time of the MOSFET and there is also option for negative bias on the V_{EE2} to prevent false turn on during high dV/dT. In Table 3-3 the electrical specification for the chosen driver circuit is stated [18].

In the datasheet for the driver circuit [18], suggested design procedures are stated. To achieve reliable performance the manufacturer recommends MLCC capacitors in parallel with the input and output voltage. It is also stated that if power supplies are far away from circuit the use of electrolytic or tantalum capacitors is needed for stabilization. To ensure that the PWM signal is stable it is recommended to add a low pass filter connected with to the drive circuit input. With consideration to manufacturers recommendations, chosen values for these components can be seen in Table 3-4.

Table 3-3 Electrical specifications for UCC5390SC

Name	Unit	Amount
UCC5390SC		
Vin	V	3.3
Vout	V	12
Iin (Icc1)	mA	2.4
Iout (Icc2)	mA	1.8
Propagation delay	ns	60
R_{NMOS}	Ω	4.5
R_{OH}	Ω	12
R_{OL}	Ω	0.65

Table 3-4 Chosen values for UCC5390SC components

Function	Component	Value
Vcc1	Capacitor MLCC	220 nF
Input filter	Capacitor MLCC	100 pF
Input filter	Resistor SMD	47 Ω
Vcc2	Capacitor MLCC	220 nF
3.3 V stabilizer	Capacitor electrolyte	10 uF
12 V stabilizer	Capacitor electrolyte	10 uF

3.3.3 -5 V Converter

In the datasheet for the gate driver UCC5390SC it is stated that there is a function for undervoltage lockout to prevent the voltage from being too low [18]. Since the 12 V battery has a V_{MIN} of 10.4 V a -5 V converter is needed to prevent this behavior. The chosen converter is the integrated circuit LT1054 from Texas Instruments and it was chosen due to availability from another project and being sufficient for the application [19].

The output of the -5 V converter will be connected to the V_{EE2} pin of the gate driver and this will affect the switching properties. By having negative bias, the voltage will rise from -5 V to 12 V when switching instead of 0 V to 12 V which leads to somewhat longer turn-on delay, but rise times are same. However, it also provides a safety margin for accidental turn on. To make sure the IC works correctly the manufacturer provides recommendations in the datasheet for design considerations. Following the design suggestions, the component values in Table 3-5 were chosen [19].

Table 3-5 Chosen values for LT1054 circuit components

Name	Component	Value
Cin	Capacitor tantalum	10 uF
C1	Capacitor MLCC	2.2 nF
R1	Resistor SMD	22 kΩ
R2	Resistor SMD	120 kΩ
Cout1	Capacitor MLCC	1 uF
Cout2	Capacitor tantalum	10 uF

3.3.4 Bootstrap

Since the upper transistor is not connected to ground it needs a bootstrap circuit to have a floating ground. The bootstrap circuit contains of a resistor, capacitor and a diode. The design of the bootstrap capacitor was based on the suggestions by Allegro in their datasheet for a MOSFET controller [20]. They stated that the bootstrap capacitor should neither be too big or too small to prevent wasting time. By using a reasonable factor of 20 times higher charge the formula for the bootstrap capacitor is

$$C_{BOOT} = \frac{Q_{GATE} \cdot 20}{V_{BOOT}} = \frac{100 \cdot 10^{-9} \cdot 20}{12} = 167 \text{ nF} \qquad (3\text{-}3)$$

Where the Q_{GATE} is the gate charge of the MOSFET and the $V_{BOOT\,is}$ the 12 V connected from the battery. A capacitor of 220 nF was chosen to have some margin.

When designing the bootstrap resistor, it is important for it to have a small resistance to shorten the time of charging the capacitor. The resistor therefore also needs to withstand large energy pulses during short periods of time. The thick film resistor RCL12181R00FKEK by Vishay of 1 Ω was chosen since it can withstand continuous pulses of over 100 W for 1 µs [21].

The proposed bootstrap diode is the CDBC5150-HF from Comchip Technology which was decided due to high efficiency, fast switching and a reverse voltage of 150 V [22]. This is important to withstand potential voltage spikes. It also has low forward voltage and can withstand the pulse of high current when charging the bootstrap capacitor.

3.3.5 Inductor

The design choices for the inductor in the DC/DC converter are limited by frequency and high current. The inductor should be able to operate at 40 A with a switching frequency of 50 kHz. According to [5] ferrite is a good choice at frequencies higher than 10 kHz due to small eddy current losses. The specification stated that the output ripple current should not exceed 15% of I_{out} which means that the inductor should not produce a larger ripple than 6 A. Following the suggested design calculations from Texas Instruments [7] using equation (2-34)

$$L > \frac{Vout \cdot (Vinmax - Vout)}{K_{ind} \cdot Fsw \cdot Vinmax \cdot Iout} = \frac{12 \cdot (60.8 - 12)}{0.15 \cdot 50000 \cdot 60.8 \cdot 40} = 32\mu H \qquad (3\text{-}4)$$

where V_{inmax} is 60.8 V, V_{out} is 12 V, I_{out} is 40 A ,F_{sw} is 50 kHz and K_{ind} is 0.15 as in the 15% current ripple. For boost mode equation (2-35) is used

$$L > \frac{Vinmin^2 \cdot (Vout - Vinmin)}{K_{ind} \cdot Fsw \cdot Iout \cdot Vout^2} = \frac{12^2 \cdot (48 - 12)}{0.15 \cdot 50000 \cdot 10 \cdot 48^2} = 30\ \mu H \qquad (3\text{-}5)$$

where V_{inmin} for boost is 12 V, V_{out} is 48 V and I_{out} is 10 A. This results in the inductor needing to have a value of at least 32 µH for this application.

An inductor that suited this specification was unfortunately not available at the suppliers and therefore it was decided to buy a magnetic core and wind the copper wire by hand. A ferrite core of the material N27 was proposed due to its optimal frequency at minimum 25 kHz and maximum 150 kHz while also being available at the suppliers [23]. In Table 3-6 the dimensions from the selected inductor datasheet is shown [23]. By using equations from chapter 2.3.1 the calculated values in Table 3-6 are stated. The limitation was that the magnetic flux density should not exceed 320 mT to keep the permeability μ_r larger than 1500 H/m. The chosen core has an air gap of 2.6 mm which will also limit the magnetic flux density given equation (2-36) which results in a limitation to the magnetic flux, using equation (2-37)

$$\Phi = \frac{B}{A_e} = \frac{320}{570 \cdot 10^9} = 182\ \mu Wb \qquad (3\text{-}6)$$

which limits the amount of turns by a maximum using equation (2-38)

$$N = \frac{\Phi \cdot R_{tot}}{I} = \frac{182 \cdot 10^{-6} \cdot 3390729}{50} = 12.34\ \text{turns} \qquad (3\text{-}7)$$

where the current is set to 50 A as a safety measure. With the decided amount of turns to be 12 the inductor value of L is calculated by equation (2-39)

$$L = \frac{N^2}{R_{tot}} = \frac{12^2}{3390729} \approx 42\ \mu H \qquad (3\text{-}8)$$

which fulfilled the condition of being larger than 32 µH.

The design of the conductor was with consideration to high current which in to have a large amount of Litz threads to increase decrease the power losses. The total cross section area of the copper wire A_{cu} was decided to be larger than 5.3 mm^2 to limit the power losses and to handle the specified current of 40 A. The used Litz strand had a diameter of 0.25 mm leading to the strand area being

$$A_z = \frac{\pi}{4} \cdot 0.25^2 \approx 0.05 \text{ mm}^2 \quad (3\text{-}9)$$

where the use of 120 Litz strands is used to satisfy an area larger than 5.3 mm^2 with some safety margin. With 120 Litz strands the total cross section area of the copper wire is

$$A_{cu} = A_z \cdot z = 0.05 \cdot 120 = 5.89 \text{ mm}^2 \quad (3\text{-}10)$$

by using equation (2-41). Which concludes in the current density

$$J_{rms} = \frac{I_{RMS}}{A_{CU}} = \frac{40}{5.89} = 6.79 \text{ A/mm}^2 \quad (3\text{-}11)$$

by using the current RMS of 40 A from the specification. The selected inductor and proposed conductor the resulting fill factor is calculated as

$$k_{cu} = \frac{N \cdot A_{cu}}{A_w} = \frac{12 \cdot 5.89}{385.77} = 0.18 \quad (3\text{-}12)$$

where the cross-sectional area for the conductor is given by

$$A_w = W_w \cdot (D_t - D_e) = 16.7 \cdot (48.8 - 25.7) = 385.77 \text{ mm}^2 \quad (3\text{-}13)$$

where the dimensions W_w, D_t and D_e are given in the datasheet, seen in Table 3-6

Table 3-6 Dimensions and calculations for selected inductor ferrite core

Dimensions	Ie	109	mm	Calculated	N	12	turns
	Ae	570	mm2		Ag	629	mm2
	Ve	62000	mm3		Rcore	101450	H^{-1}
	De	25.7	mm		Rgap	3289279	H^{-1}
	Dt	48.8	mm		Rtot	3390729	H^{-1}
	Wc	62	mm		Φ	1.8E-04	Wb
	g	2.6	mm		B	310.4	mT
	Ww	16.7	mm		L	42.47	mH
	Wt	24.5	mm				

3.3.6 Power Losses

The DC/DC converter will have the majority of the power losses in the inductor as well as the MOSFETs. The power losses are divided into two sections for the components, core and winding losses for the inductor, switching and conduction for the MOSFET. Some additional power losses will appear in the -5 V converter and in the driver stage. To prepare the needed heatsink the power losses are calculations after worst case.

With the chosen MOSFET we get the following conduction power losses

$$P_{on-boost} = r_{on} I_{on}^2 \frac{t_{on}}{Ts} = 4.4 \cdot 10^{-3} \cdot 40^2 \cdot 0.75 = 5.28\ \text{W} \quad \textit{(3-14)}$$

for the boost MOSFET with a duty cycle of 75% and the following for the buck MOSFET

$$P_{on-buck} = r_{on} I_{on}^2 \frac{t_{on}}{Ts} = 4.4 \cdot 10^{-3} \cdot 40^2 \cdot 0.25 = 1.76\ \text{W} \quad \textit{(3-15)}$$

with a duty cycle of 25%. These calculations are for worst case situation when conducting 40 A. The switching with a switching frequency of 50 kHz the power losses are calculated using equation (2-28)

$$P_s = 0.5 \cdot 48 \cdot 10 \cdot 50000 \cdot (210\ \text{ns} + 141\text{ns}\ + 17\text{ns} + 112\text{ns}) = 5.77\ \text{W} \quad \textit{(3-16)}$$

where the values for V_d and I_o are considered to be from the 48 V battery. The switching times are calculated with the maximum values from MOSFET datasheet [17] and with consideration to the chosen driver circuit resistances and the external gate resistances. With the chosen external resistances of R_{extoff} of 5.6 Ω and R_{exton} of 33 Ω the total gate resistance is

$$R_{gon} = R_{exton} + R_{NMOS} || R_{OH} = 33 + \frac{12 \cdot 4.5}{12 + 4.5} = 36.2727\ \Omega \quad \textit{(3-17)}$$

$$R_{goff} = R_{extoff} + R_{OL} = 5.6 + 0.65 = 6.25\ \Omega. \quad \textit{(3-18)}$$

The total power losses from the MOSFETs concludes in

$$P_{MOSFET} = P_{on-boost} + P_{on-buck} + 2 \cdot P_{sw} = 5.28 + 1.76 + 2 \cdot 5.77 = 18.58\ \text{W} \quad \textit{(3-19)}$$

where the switching losses are assumed to be the same for both MOSFETs.

The other big contributor of power losses is the inductor, the winding losses produced by the chosen inductor is calculated to be

$$P_w\ =\ \rho \cdot k_{cu} \cdot J_{rms}^2 \cdot V_w = 22 \cdot 10^{-9} \cdot 0.18 \cdot 6.79^2 \cdot 45144 \cdot 1000 = 8.4\ \text{W} \quad \textit{(3-20)}$$

where the used I_{RMS} is set to be 40 A and $\rho$is the resistivity of copper at 100℃. Since the core losses in the inductor are dependent on the material, the datasheet for N27 by TDK was used [23] in the third graph on page 5 the relative core losses versus frequency relationship is shown. By calculating the magnetic flux density

$$B = \Phi \cdot A_e = \frac{N \cdot I}{R_{tot}} \cdot A_e = \frac{12 \cdot 6}{3390729} \cdot 570 \cdot 10^9 \simeq 37.3 \text{ mT} \quad (3\text{-}21)$$

where the current I is the AC current through the inductor of 6 A peak to peak. In the graph it is only stated for 50 mT and therefore we get some margin of error for the core losses. The P_V is stated to be 20 kW/m^3 for a magnetic flux density of 50 mT at a switching frequency of 50 kHz. Hence the power loss is

$$P_{core} = V_e \cdot P_V = \frac{62000}{10^9} \cdot 20000 = 1.24 \text{ W} \quad (3\text{-}22)$$

where V_e is the magnetic core volume given in mm^3. The total inductor losses are then

$$P_{INDUCTOR} = P_{core} + P_w = 8.4 + 1.24 = 9.64 \text{ W} \quad (3\text{-}23)$$

Lastly the power losses from the -5 V converter and the driver circuit. The converter power losses are calculated with the formula given in the datasheet [19]

$$P_{-5V} = (V_{cc} - V_{OUT}) \cdot I_{OUT} + V_{CC} \cdot I_{OUT} \cdot 0.2 \quad (3\text{-}24)$$

where V_{CC} is the 12 V from the Arduino, V_{OUT} is the -5 V output from the converter and I_{OUT} will provide the gate charge, calculated as

$$I_{OUT} = Q_{GD} \cdot f_{sw} = 24 \cdot 10^{-9} \cdot 50000 = 1.2 \text{ mA} \quad (3\text{-}25)$$

which means that the power loss from the -5 V converter will be

$$P_{-5V} = (12 - (-5)) \cdot 1.2 \cdot 10^{-3} + 12 \cdot 1.2 \cdot 10^{-3} \cdot 0.2 = 23 \text{ mW}. \quad (3\text{-}26)$$

The power losses from the driver circuit is based on the proposed estimation in the datasheet [18]. The losses are calculated by

$$P_{GDQ} = V_{CC1} \cdot I_{VCC1} + V_{CC2} \cdot I_{VCC2} = 3.3 \cdot 2.4 + 12 \cdot 1.8 = 29.52 \text{ mW} \quad (3\text{-}27)$$

where V_{CC1} is the 3.3 V from the Arduino power supply and I_{CC1} is the current provided, stated as maximum of 2.4 mA in the datasheet. V_{CC2} is the 12 V battery and I_{CC2} is battery supply current of maximum 1.8 mA. According to the datasheet the other component of power loss is from the switching, given by

$$P_{GSW} = V_{CC2} \cdot Q_G \cdot f_{SW} = 12 \text{ V} \cdot 100 \text{ nC} \cdot 50 \text{ kHz} = 60 \text{ mW} \quad (3\text{-}28)$$

where V_{CC2} is the 12 V battery, Q_G is the MOSFET gate charge and f_{SW} is the switching frequency. It is stated in the datasheet that if external resistances are used the equation for the switching losses needs to be adjusted. To include the losses in the external gate resistances the following equation should be used

$$P_{GDO} = \frac{P_{GSW}}{2} \cdot \left(\frac{R_{OH} || R_{NMOS}}{R_{OH} || R_{NMOS} + R_{ON} + R_{GFET}} + \frac{R_{OL}}{R_{OL} + R_{OFF} + R_{GFET}}\right) \simeq 5.4 \text{ mW} \quad (3\text{-}29)$$

where the values for R_{OH}, R_{OL}, and R_{NMOS} are stated in Table 3-4 for the driver circuit and R_{ON}, R_{OFF} are the external gate resistance of 33 Ω and 5.6 Ω. The value for R_{GFET} is the typical gate resistance of 0.8 Ω from MOSFET datasheet. The total power loss for the driver is then

$$P_{DRIVER} = P_{GDQ} + P_{GDO} = 29.52\ \text{mW} + 5.4\ \text{mW} \simeq 35\ \text{mW} \qquad (3\text{-}30)$$

giving us the total power losses in the system to be

$$P_{loss-total} = P_{MOSFET} + P_{INDUCTOR} + P_{-5V} + P_{DRIVER} = 18.58 + 9.64 + 0.023 + 2 \cdot 0.035 = 28.313\ \text{W} \qquad (3\text{-}31)$$

which indicates that the circuit will generate a lot of heat. This calculation will be used as a basis when designing the heat sink for the system.

3.3.7 Thermal Considerations

In order to understand the heat flow in the power electronic circuit a heat flow diagram can be seen in Figure 3-8. An equivalent circuit representing the heat flow from the switches to the ambient air can be seen in Figure 3-9. During the project it was decided that the inductor is placed outside the PCB and therefore is not included in the calculations.

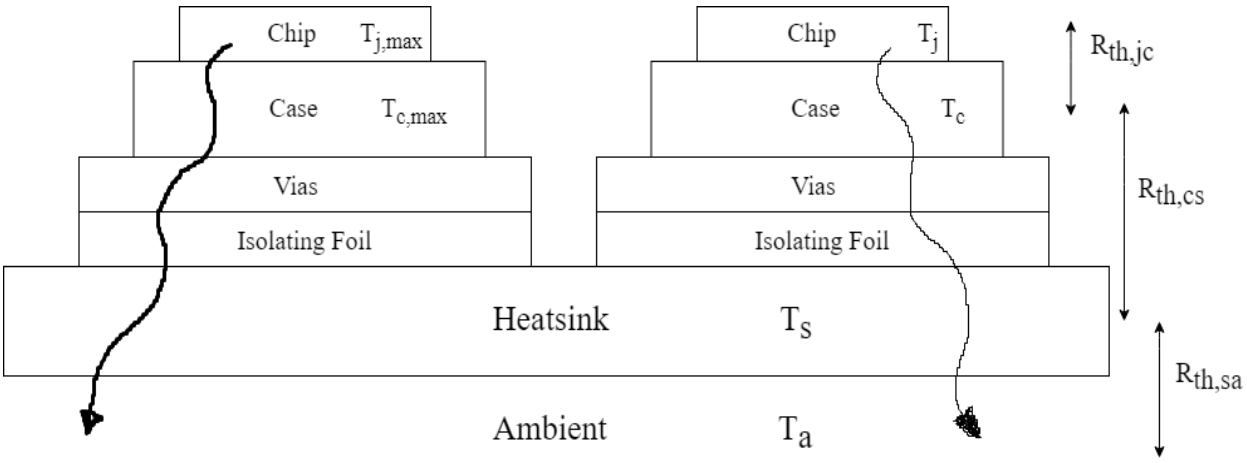

Figure 3-8 Heat flow diagram

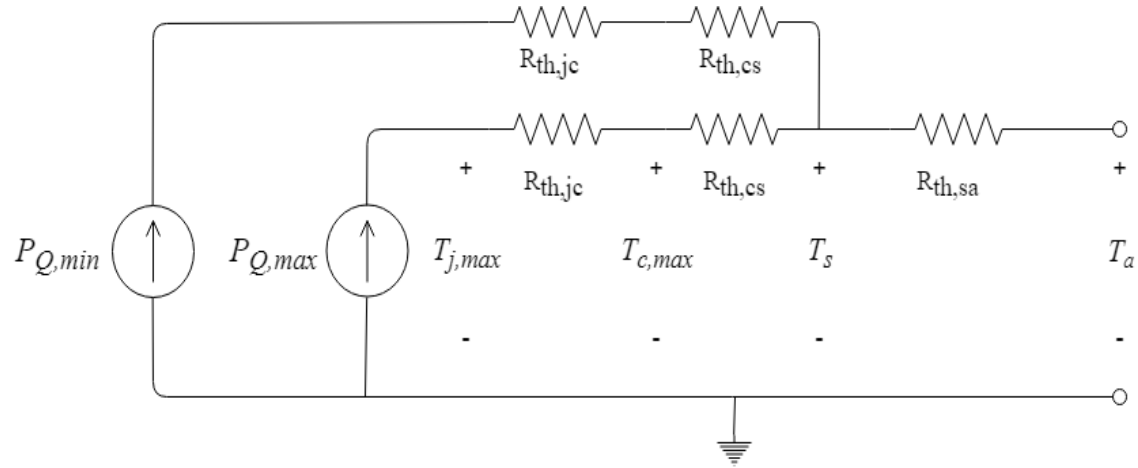

Figure 3-9 Equivalent heat flow circuit

To calculate a suitable heatsink for this system a desired value of the maximum junction temperature $T_{j,max}$ is chosen to 80 ℃ and ambient temperature T_a 30 ℃, which gives a case temperature of 72.5 ℃, which is acceptable. The power dissipated is approximated from the calculated values with an added safety margin where the total power dissipated from the MOSFETs, P_{tot}, is chosen to 20 W. In order to calculate the worst case maximum junction temperature, the maximum power dissipated from a single MOSFET P_{Qmax} is assumed to be 15 W. The junction to case thermal resistivity $R_{th\ jc}$ can be found in the MOSFETs datasheet and is 0.5 W/°K. The case to heatsink thermal resistivity is

$$R_{th\ cs} = R_{th\ foil} + R_{th\ pad} = 0.12 + 0.47 = 0.59\ \text{W/°K} \tag{3-32}$$

where $R_{th\ foil}$ is the thermal resistivity of the isolating thermal foil which lies pressed between the heatsink and the vias on the opposite side of the MOSFETs on the PCB. $R_{th\ pad}$ is the thermal resistivity of the vias that the MOSFETs are placed on and is calculated using the online PCB via calculator [24].

Using the formula (2-46) the maximum thermal resistivity of the heatsink, $R_{th\ sa}$, can be calculated as

$$R_{th\ sa} = \frac{[\![(T]\!]_s - T_a)}{P_{tot}} = \frac{T_{c,max} - \left(R_{th\ cs} * P_{Q\ max}\right) - T_a}{P_{tot}} = \frac{\left(T_{j,max} - \left(R_{th\ jc} * P_{Q\ max}\right)\right) - \left(R_{th\ cs} * P_{Q\ max}\right) - T_a}{P_{tot}} \tag{3-33}$$

$$R_{th\ sa} = ((80 - (0.5 * 15)) - (0.59 * 15) - 80)/20 = 1.6825\ \text{W/°K}.$$

Choosing a heatsink with a thermal resistivity $R_{th\ sa}$ of 1.5 W/°K the maximum junction temperature $T_{j,max}$ can be calculated as

$$T_{j,max} = T_{c,max} + (R_{th\ jc} * P_{Q\ max}) = T_s + (R_{th\ cs} * P_{Q\ max}) + (R_{th\ jc} * P_{Q\ max})$$

$$T_{j,max} = T_a + (R_{th\ sa} + P_{tot}) + \left(R_{th\ cs} * P_{Q\ max}\right) + \left(R_{th\ jc} * P_{Q\ max}\right) \tag{3-34}$$

$$T_{j,max} = 30 + (1.5 + 20) + (0.59 * 15) + (0.5 * 15) = 76.35\ ℃.$$

3.3.8 PCB Design

A design of the PCB was made using Ultiboard. Figure 3-10 shows an image of the complete control system, where the leftmost part (in blue square) is contains the footprints and traces for the components needed for the bidirectional DC/DC converter that is the focus in this report. The rightmost part (in grey square) contains footprints and traces for the components for the inverter needed to drive the BLDC motor from the 48 V battery.

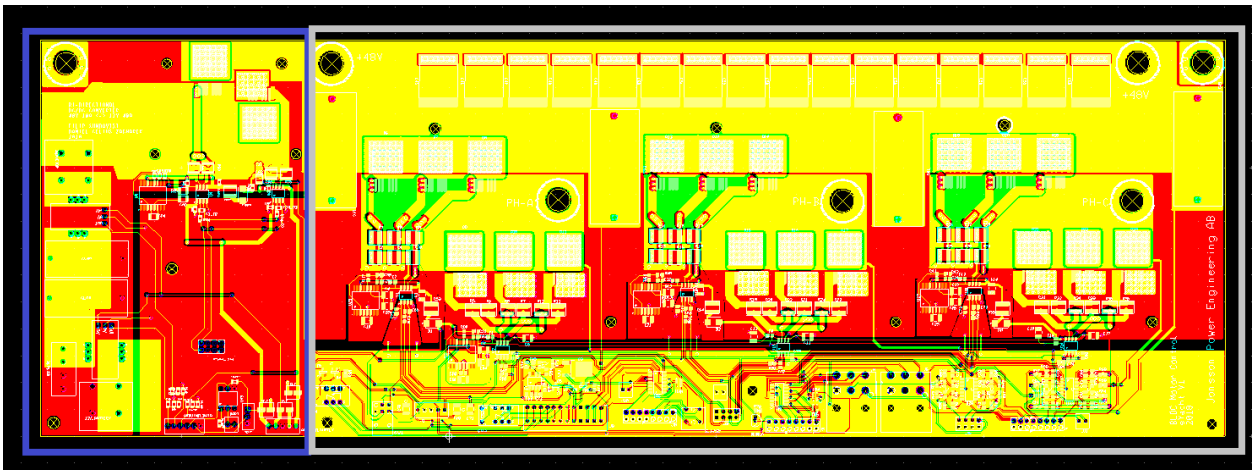

Figure 3-10 PCB design for DC/DC converter (in blue square) and BLDC inverter (in grey square)

When placing the components footprints on the board it is important to consider the thermal design. Since a surface mounted power transistor is to be used, the through-hole components must be placed on the edges of the PCB to provide adequate room for the heatsink to be mounted below the power transistors as the heatsink is pressed against a thermal pad that lies on a matrix of vias that will conduct the heat from the transistor to the heatsink. This also requires that all other components that should be placed close to the transistors are surface mounted devices as well to isolate them from the heatsink.

It is also important to consider how stray inductances from the traces needed to connect components will affect components. Picking components that are surface mounted and placing them close together can help minimize these inductances. Traces that will have a large current flowing through them need to be made wider to reduce resistance and thus losses. Figure 3-11 shows a closeup of the PCB design for the DC/DC converter where the width of the traces are calculated using the trace width calculator [25] that recommended 45 mm width for 40 A traces and 10 mm for 10 A traces.

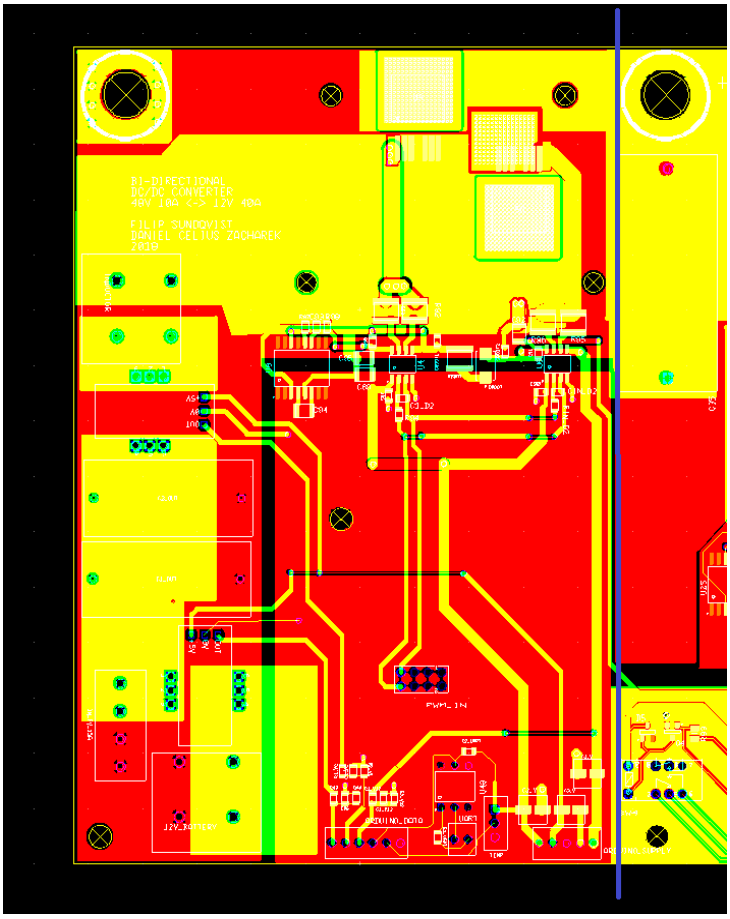

Figure 3-11 Closeup of PCB design for DC/DC converter (left of blue line)

3.4 Microcontroller and Software

The microcontroller in the system that will control the PWM, partial integrator (PI) regulator, the battery management system and the BLDC motor is an Arduino Due. It contains of an Atmel SAM3X8E ARM Cortex-M3 32-bit CPU and 54 digital inputs/output pins of which 12 can be used as PWM outputs. It also contains 12 analog inputs and 4 UARTs (Universal Asynchronous Receiver-Transmitter). The maximum clock speed is 84 MHz and there is 512 Kb flash and 100 Kb SRAM [26].

The system requires multiple signals in order to work properly. The duty cycle for the MOSFETs on the converter needs to be controlled to transfer the desired power. The temperature needs to be observed to not break components. The voltage and current of each battery needs to be measured to verify that they are at proper levels, if not, regulate them with the PI regulator. By measuring the voltage and current the SoC will be calculated using coulomb counting to decide the mode of operation [9].

3.4.1 Inputs

For the software to operate it will need different input signals from the circuit in order to produce control signals. The signals from the circuit are: inductor current to the 12 V battery, total current to the 12 V battery, including the current provided by the PV panels, voltage measurement of the 12 V battery, ambient temperature measurement, a UART signal from the 48 V battery BMS, voltage and current to the 48 V battery be received.

3.4.2 Outputs

From the input signals the output, or control signals will be calculated. The output signals are the PWM signals whose duty cycle will determine when the MOSFETs shall switch to their conducting or blocking modes. Using the Arduinos built in PWM function a 50 kHz 10-bit PWM is realized. The duty cycle will be regulated by a PI controller that requires a reference value and a desired value. Depending on the batteries SoC the different charge or discharge modes will be decided. The choosing of the operation modes are the same as the discussed in the theory for the battery management system.

3.5 Software Test

To test the software before connecting it to the real system a test-bench was made. In Table 3-7 a list can be seen consisting of the components used for testing the software. The circuit was configured as the chosen circuit topology to test both buck and boost operation with voltage and current controlled PI. This was important to make sure that regulator was fast enough before connecting two batteries together. By using both current and voltage regulated PI the functions constant current and constant voltage charge discussed in 2.7 could be tested. The software seen in Figure 3-12 was made in Simulink where interactive simulation was used in combination with the Arduino Due to test the system. The software contains of two Arduino inputs that provides the current and voltage measurements, the subsheets called PI voltage and PI current contains discrete PI regulators with chosen constants for amplifying the error. The subsheet called PWM contains a S-Function that configures the Arduino for 50 kHz PWM and chosen duty cycle.

Table 3-7 Components used during software test

Microcontroller	Arduino Due
Lead battery	12 V
Effect resistor	15 Ω
MOSFET	IRFP4468PbF
-5 V converter	LT1054
Driver circuit	UCC5390SC
Created inductor	42 μH
Current sensor	LTS 25-NP

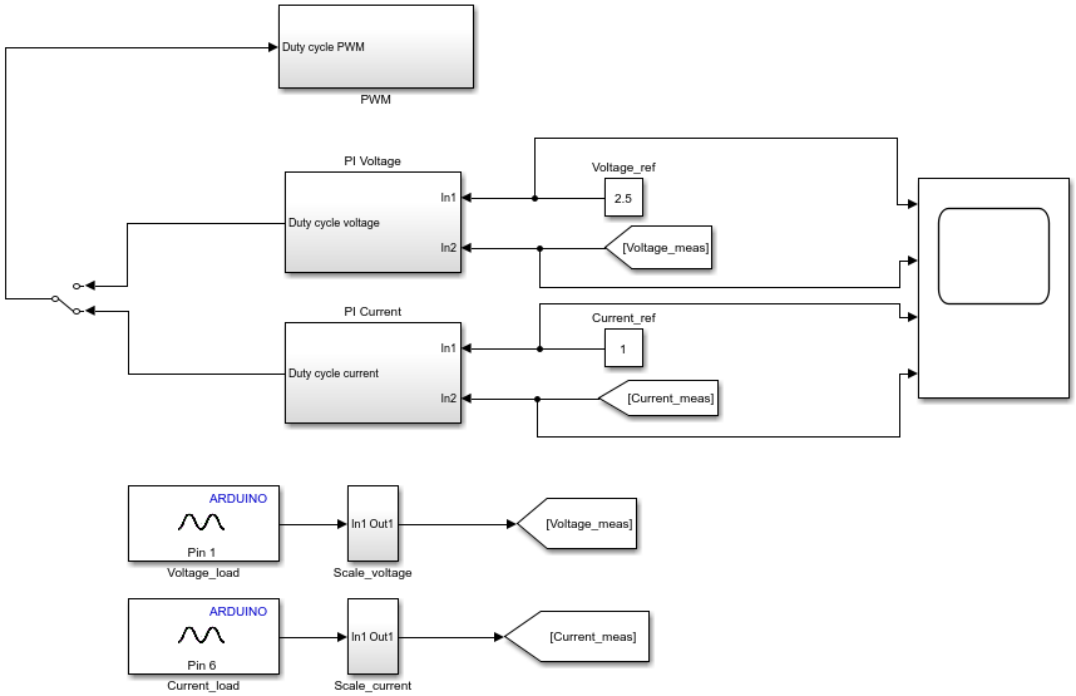

Figure 3-12 Software test in Simulink

4 Result

The results will provide the basis for the discussion and conclusion with the consequences of the method. It contains the final simulations with models for the selected components, tests of the regulating software as well as the final layout of the designed PCB.

4.1 Final System Design

The resulting design of the synchronous bidirectional DC/DC converter is shown in Figure 4-1. This circuit contains the final chosen components with selected values.

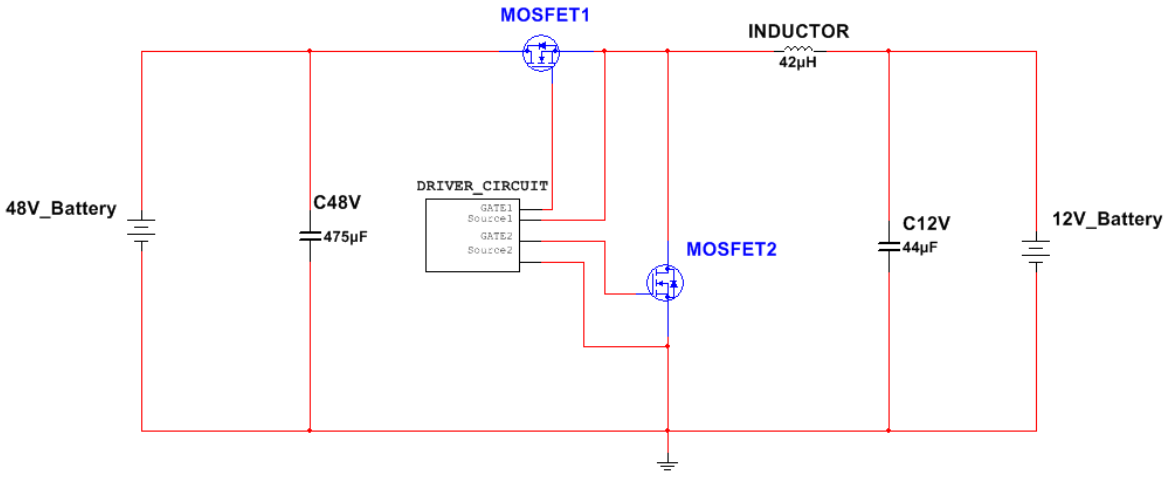

Figure 4-1 Converter circuit with capacitor and inductor values

The inside of the driver subsheet can be seen in Figure 4-2 which shows the values of the chosen components. Only one -5 V converter is needed that will be referenced to the source of the upper MOSFET. The -5 V that is required for the lower MOSFET is referenced to ground is shared from the motor inverter circuit since it already has a -5 V referenced to ground.

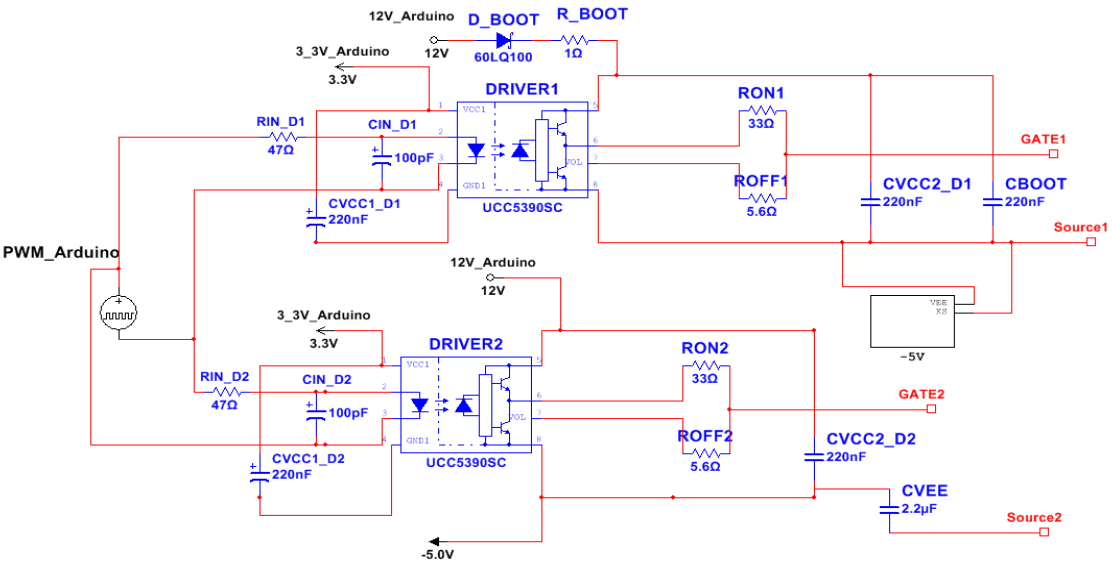

Figure 4-2 Inside the driver circuit subsheet with the final decided component values

The inside of the -5 V converter circuit subsheet with chosen component values can be seen in Figure 4-3.

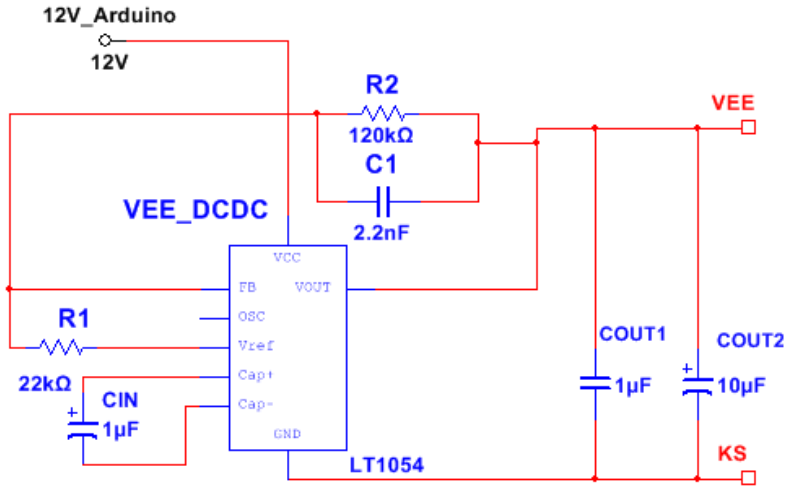

Figure 4-3 Inside of the -5 converter subsheet

4.2 MATLAB Simulink

The simulation of the topology with the chosen values can be seen in Figure 4-4. The values for the components is an inductor of 42 µH, the DC bus capacitors of 470 µF on the 48 V side and a capacitor of 44 µF on the 12 V side. The simulation also consists of the PI regulator that will be implemented in the Arduino Due. The PI is fed with the error between the chosen current reference, here shown as 40 A, and the measured current through the inductor.

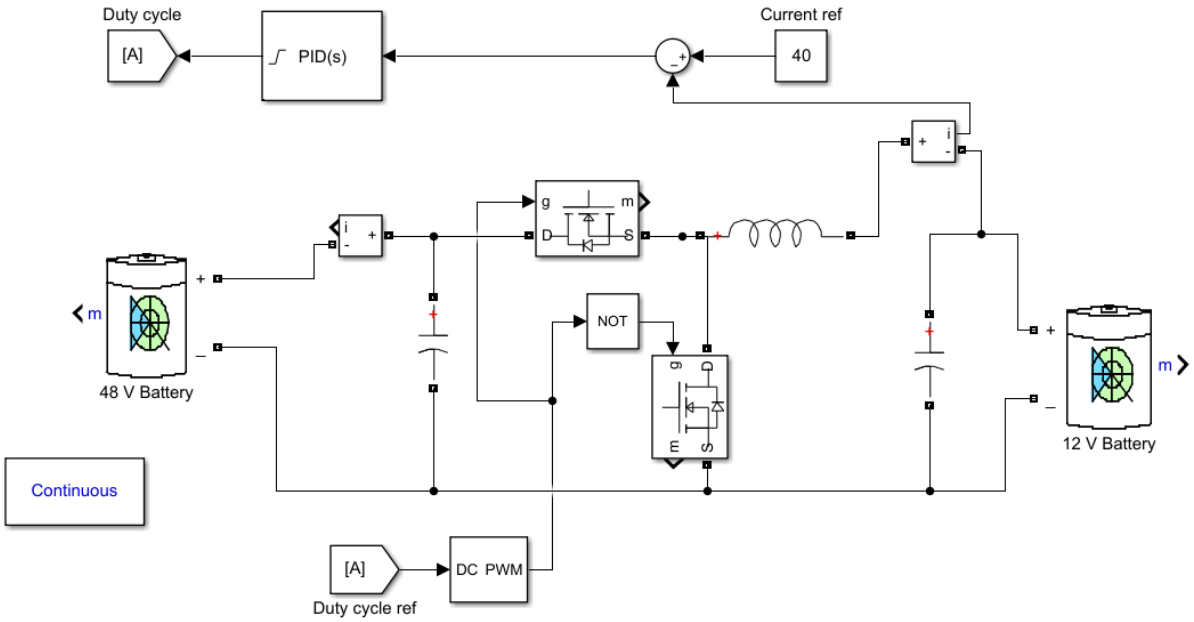

Figure 4-4 Topology simulated with PID in MATLAB Simulink

To satisfy the specification the inductor current is shown in Figure 4-5, where the current ripple is approximately 2 A.

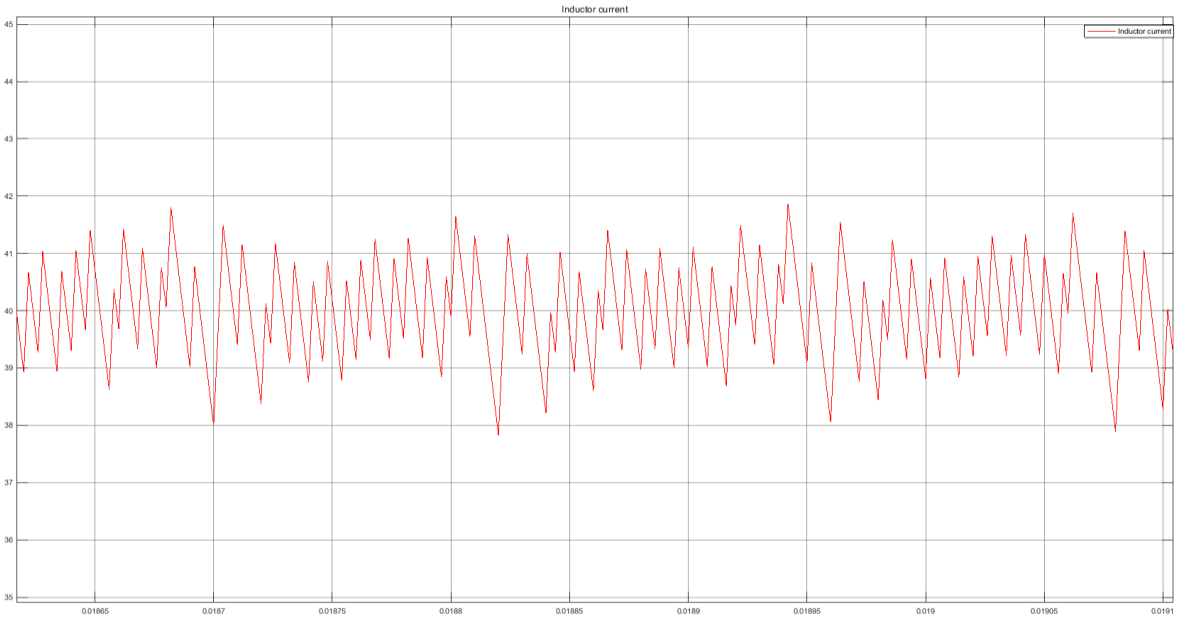

Figure 4-5 Current through inductor with a current reference of 40 A

In Figure 4-6 the voltage and current charging the 12 V battery with 40 A can be seen. The figure shows that the current charging the battery has a ripple of approximately 1.5 A and only a voltage ripple of 0.1 V. This was achieved with the 44 µF capacitor in parallel with the 12 V battery that works as a filter.

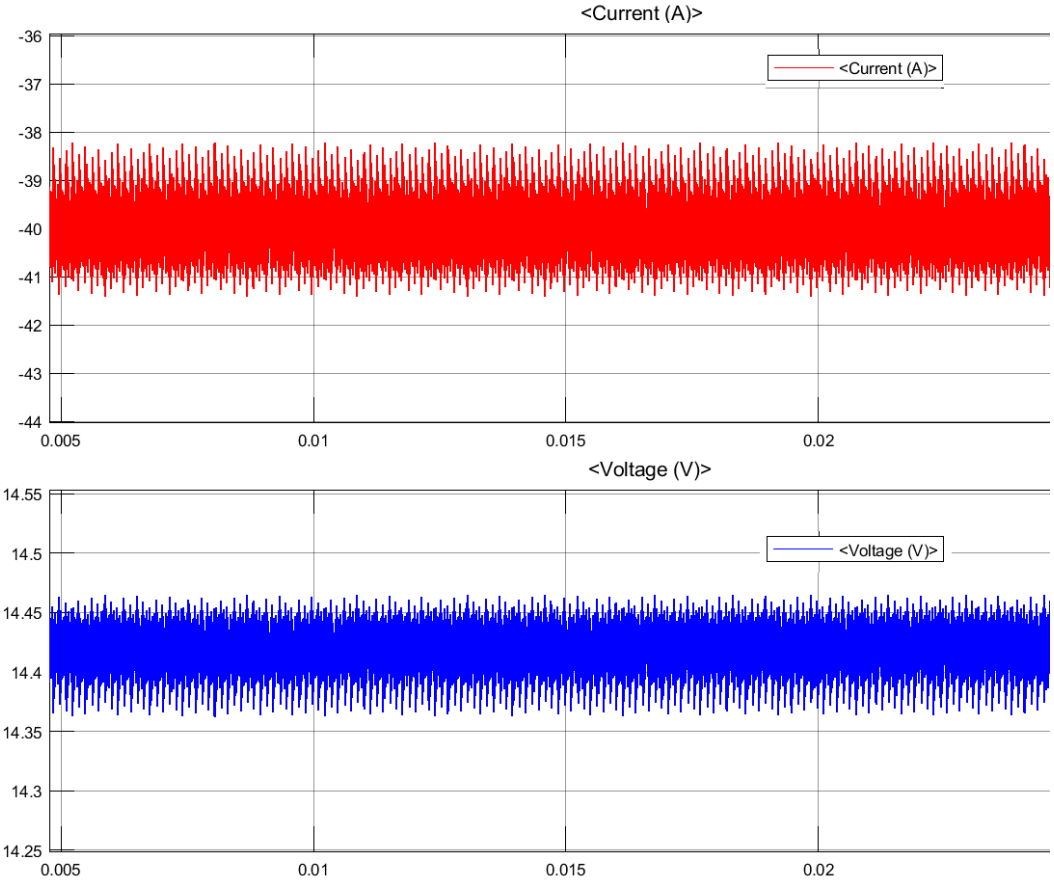

Figure 4-6 Voltage and current charging the 12V battery in MATLAB Simulink

In Figure 4-7 the voltage and current charging the 48 V battery with 10 A can be seen. A current ripple of approximately 2 A is seen and a voltage ripple of 0.15 V.

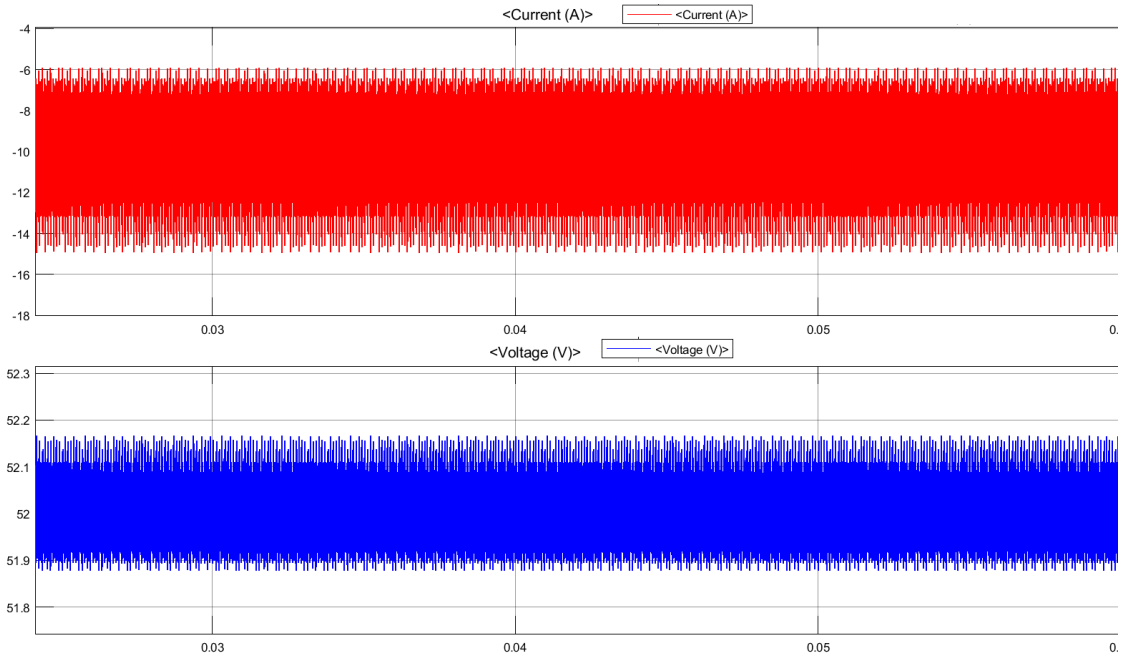

Figure 4-7 Voltage and current charging the 48 V battery in MATLAB Simulink

4.3 MultiSIM

In Figure 4-8 the final circuit designed in MultiSIM for the simulation of switching characteristics can be seen. The capacitors are based on the suggested values from Table 3-4. The bootstrap diode, resistor and capacitor are the decided values from chapter 3.3.4. As discussed in the MOSFET section 2.2.1 the values for R_{gon} and R_{goff} are of significant importance.

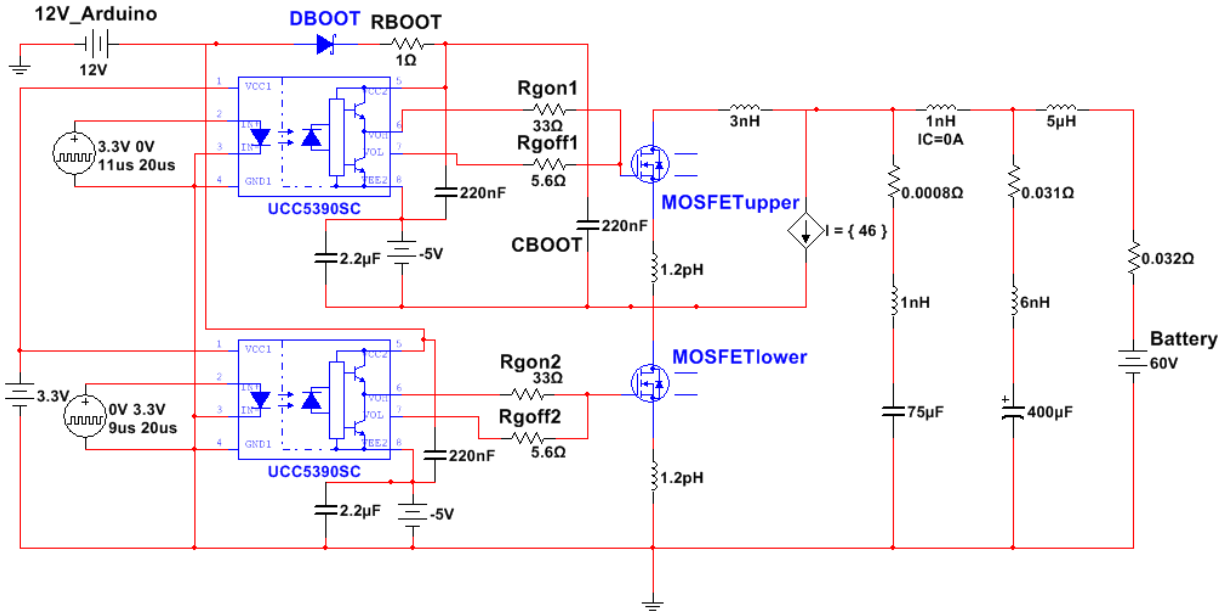

Figure 4-8 Final circuit for MOSFET simulation with decided values in MultiSIM

The result of the values 33 Ω and 5.6 Ω can be seen in Figure 4-9 where the gate-source is shown when a large dV/dT is present. The figure shows that the spikes does not exceed Vth which has a minimum of 3 V [17], which was desired. The figure also shows the importance of the -5 V converter since the gate-source voltage V_{GS} would have exceeded the threshold voltage Vth if the reference would have been ground.

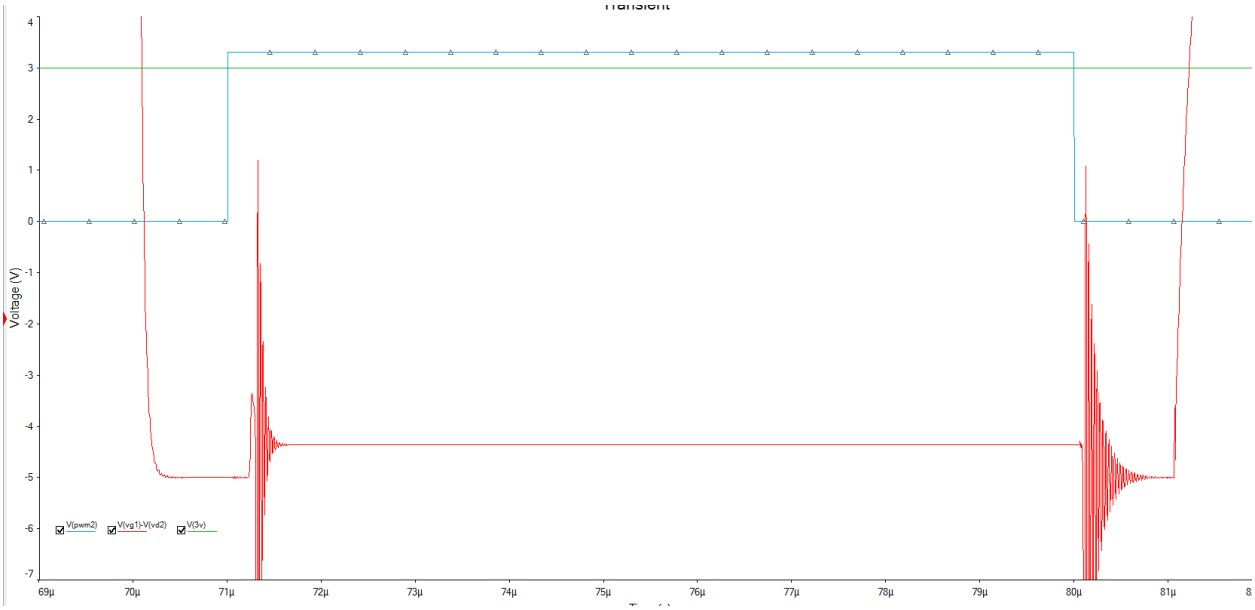

Figure 4-9 Gate-source voltage for upper transistor, limit of 3 V and PWM for lower transistor

With the -5 V converter and the decided values for the external resistances the switching characteristics were simulated to measure the resulting delay. In Figure 4-10 the turn on time can be seen for upper MOSFET and in Figure 4-11 the turn off. The resulting time for turn on is approximately 1.5 µs and the resulting time for turn off 0.3 us. This delay will affect the duty cycle but was necessary as a safety measure.

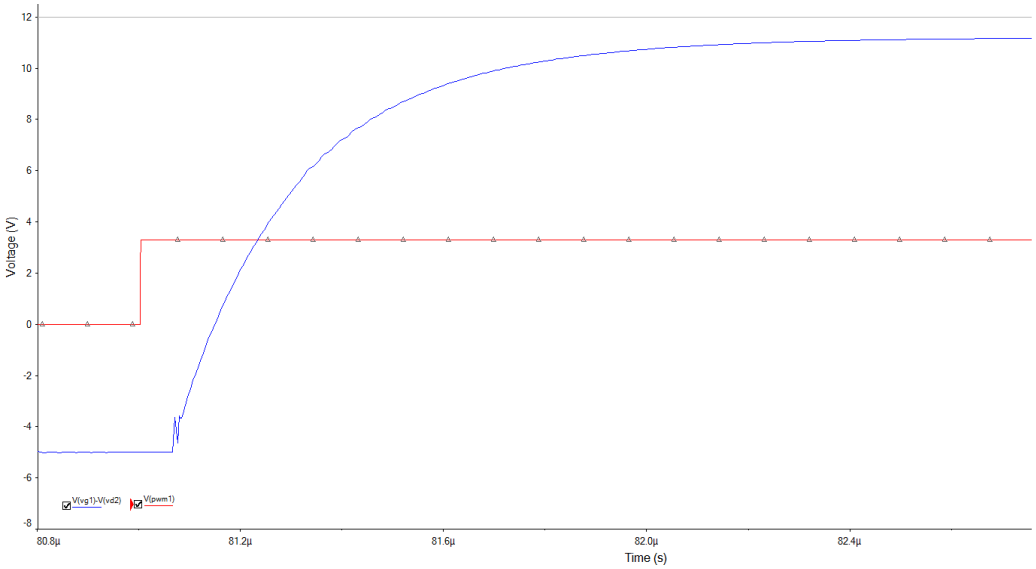

Figure 4-10 VGS for the upper MOSFET during turn on, the PWM signal can also be seen

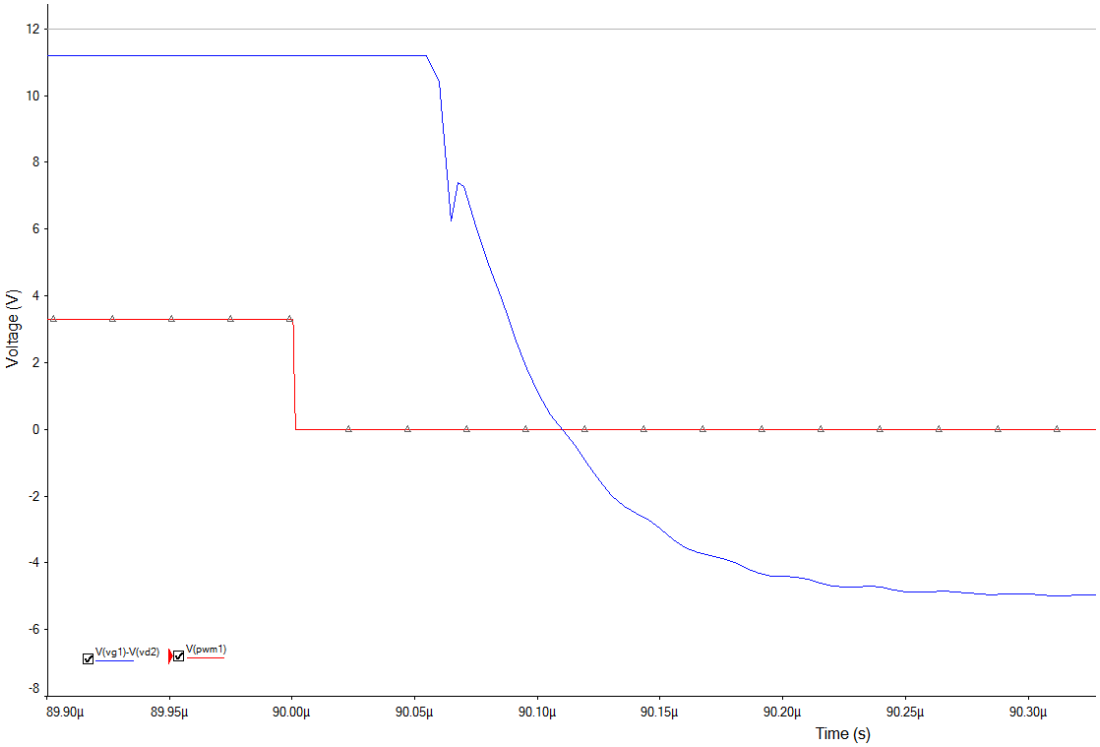

Figure 4-11 VGS for the upper MOSFET during turn off, the PWM signal can also be seen

It was stated in the specification that the voltage spike V_{DS} should not exceed 120 V. To minimize the capacitor parasitic inductances, it was chosen to use surface mounted components. This reduced the voltage spike seen in Figure 4-12 for the upper MOSFET and in Figure 4-13 for the lower MOSFET, showing that the specification is met with a voltage spike lower than 120 V.

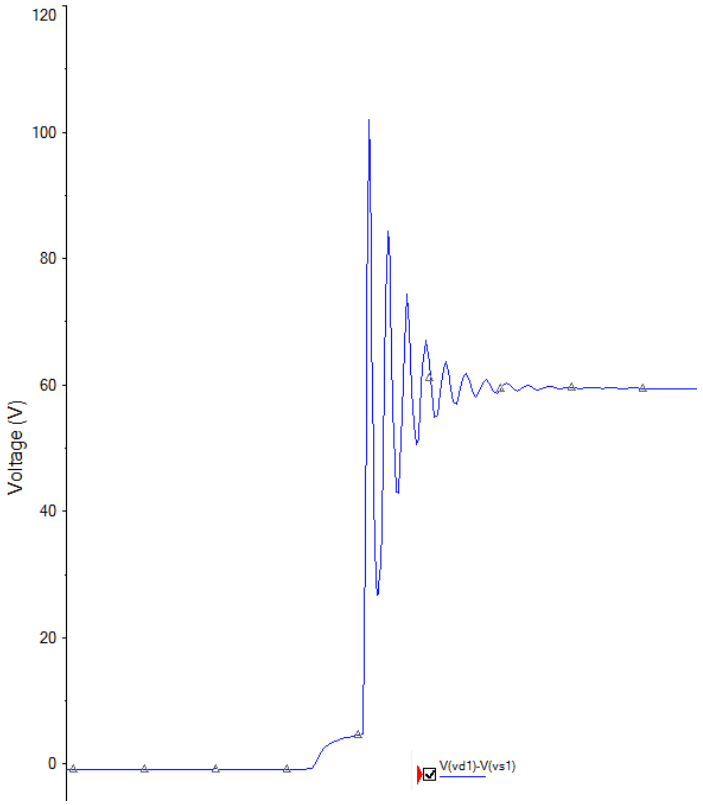

Figure 4-12 The voltage spike due to large dV/dt in upper MOSFET

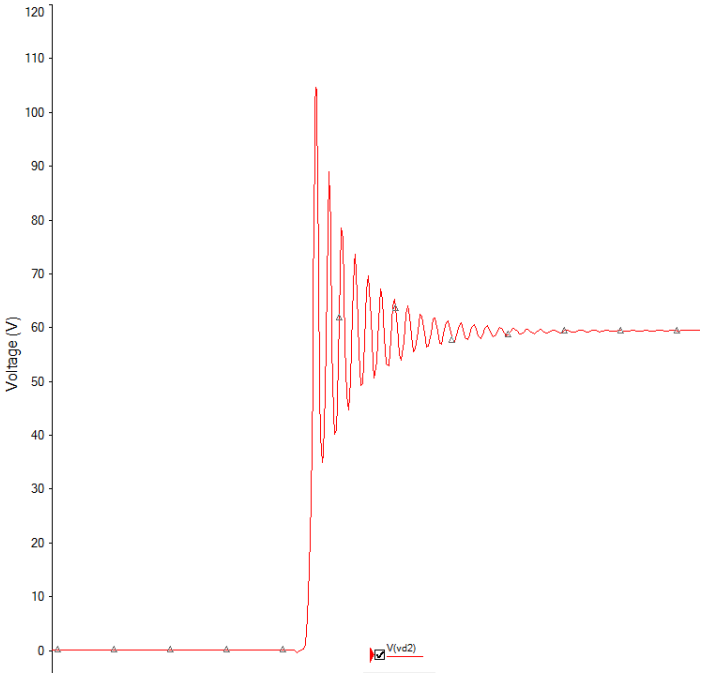

Figure 4-13 The voltage spike due to large dV/dt in lower MOSFET

4.4 Efficiency

With the power losses calculated in section 3.X the proposed efficiency can be calculated as

$$\eta = \frac{P_{OUT}}{P_{IN}} = \frac{P_{IN} - P_{loss-total}}{P_{IN}} = \frac{(12 \cdot 40) - 28.313}{12 \cdot 40} = 94.1\ \% \qquad (4\text{-}1)$$

where Pin is calculated based on the same operation as the power losses. This operation being the operation with a voltage of 12 V and a current of 40 A.

4.5 PCB

A three-dimensional image of the final PCB design can be seen in Figure 4-14. Not all footprints used in the project consists of the correct dimensions in 3D.

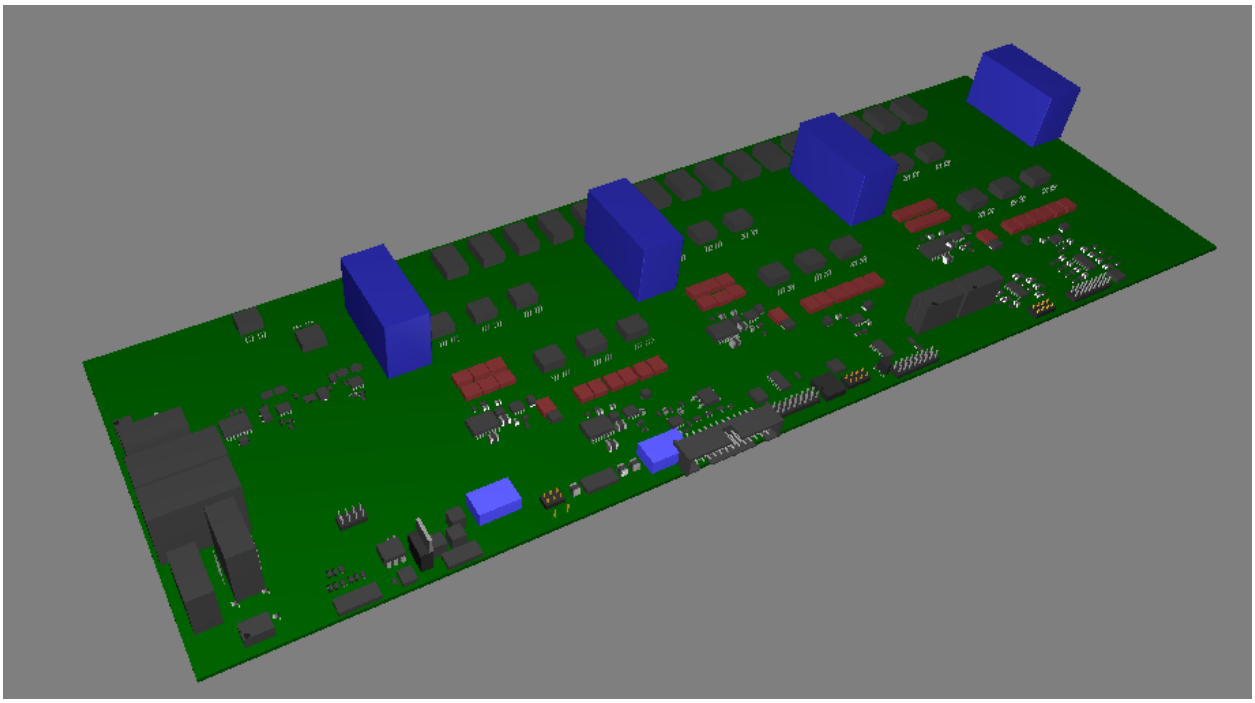

Figure 4-14 3D preview of PCB design

4.6 Software Test

To test with the Simulink software, the simulation ran in continuous mode which means that the Arduino Due and Simulink are connected during the test. Therefore, it is possible to change constants and to measure the analog signals from the Arduino with a computer. Constant current and constant voltage charge was both simulated with buck and with boost mode with the step responses documented. In all the figures the time scale is one second per square. In Figure 4-15 constant current regulation is used during boost mode when the reference current is changed from 2 A to 5 A.

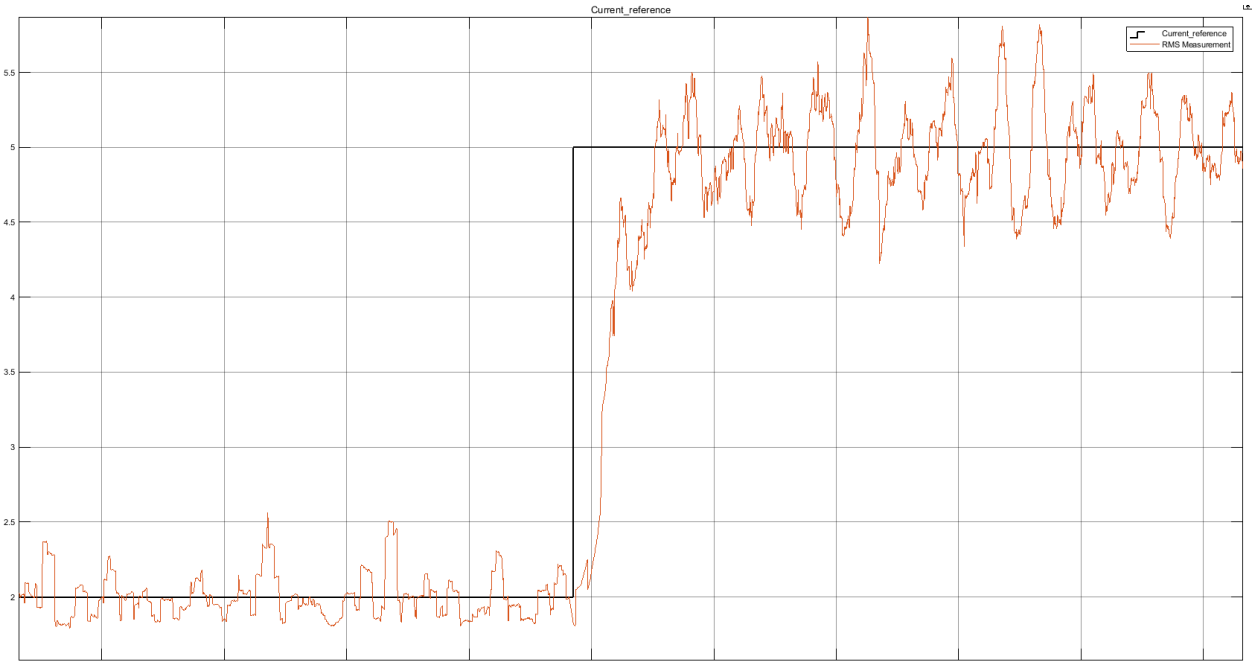

Figure 4-15 Step response of constant current regulation during boost mode (1 second per square)

The Figure 4-16 contains the step response for constant voltage regulation during boost mode when the voltage reference is changed from 5 to 10 V.

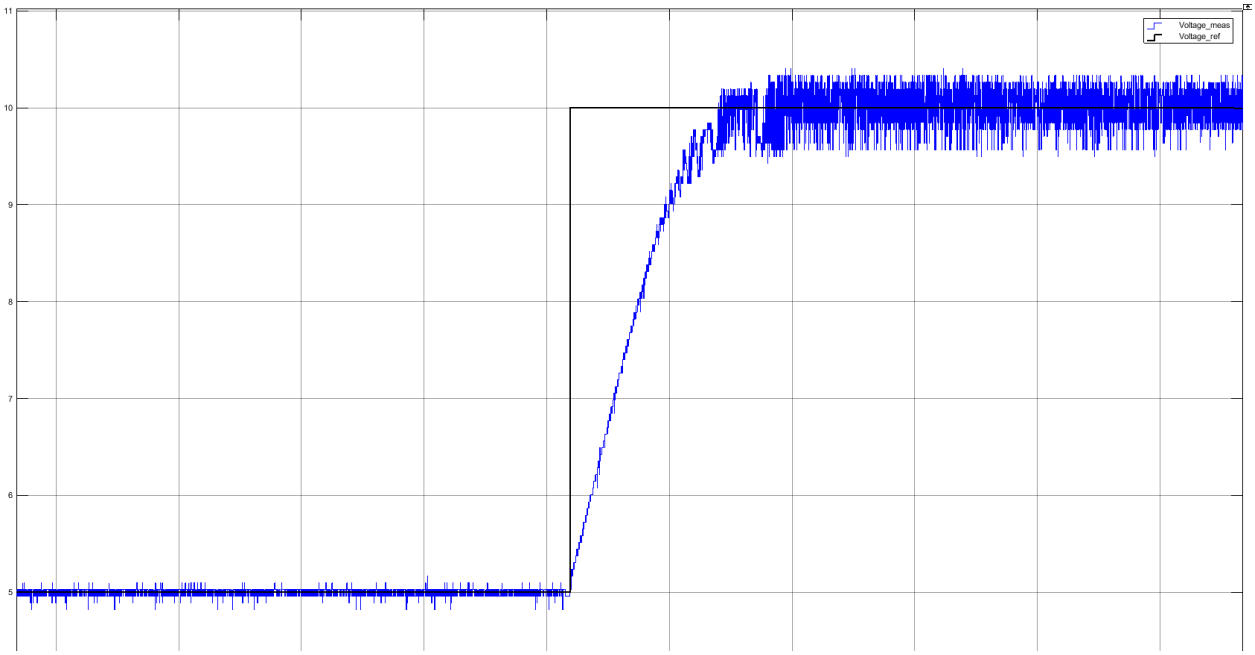

Figure 4-16 Step response of constant voltage regulation during boost mode (1 second per square)

The step response for buck mode with constant current charge can be seen in Figure 4-17 where the reference current is changed from 2 A to 1 A.

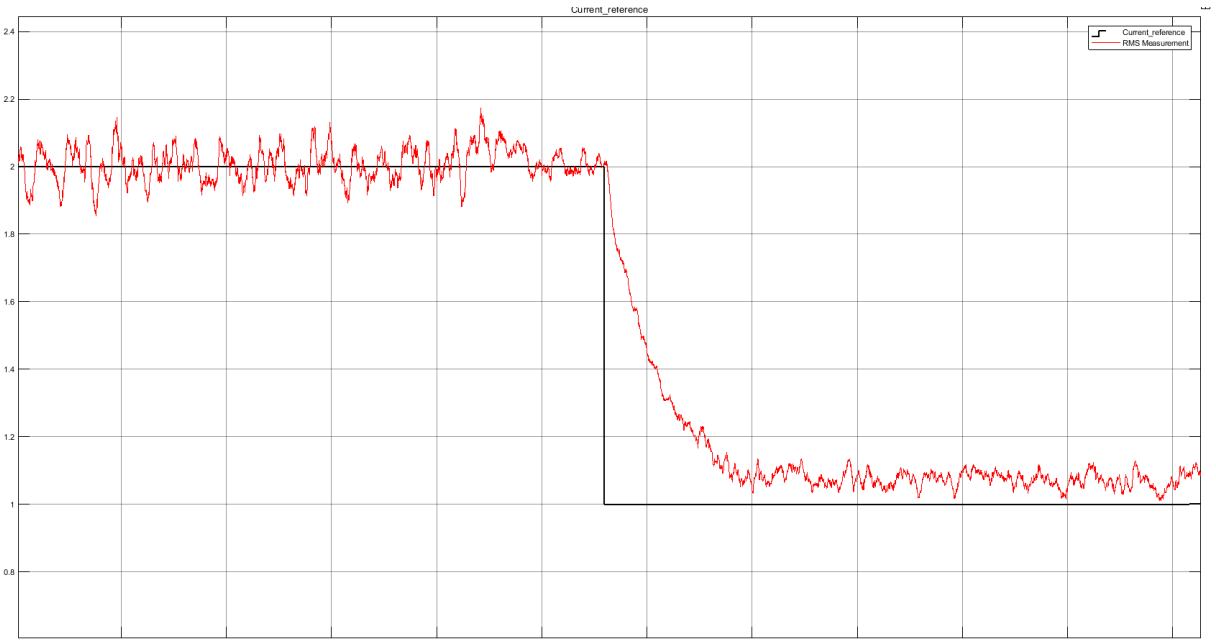

Figure 4-17 Step response of constant current regulation during buck mode (1 second per square)

The last step response can be seen in Figure 4-18 where the constant voltage regulation during buck mode changing the voltage reference is changed from 9 to 2.5 V.

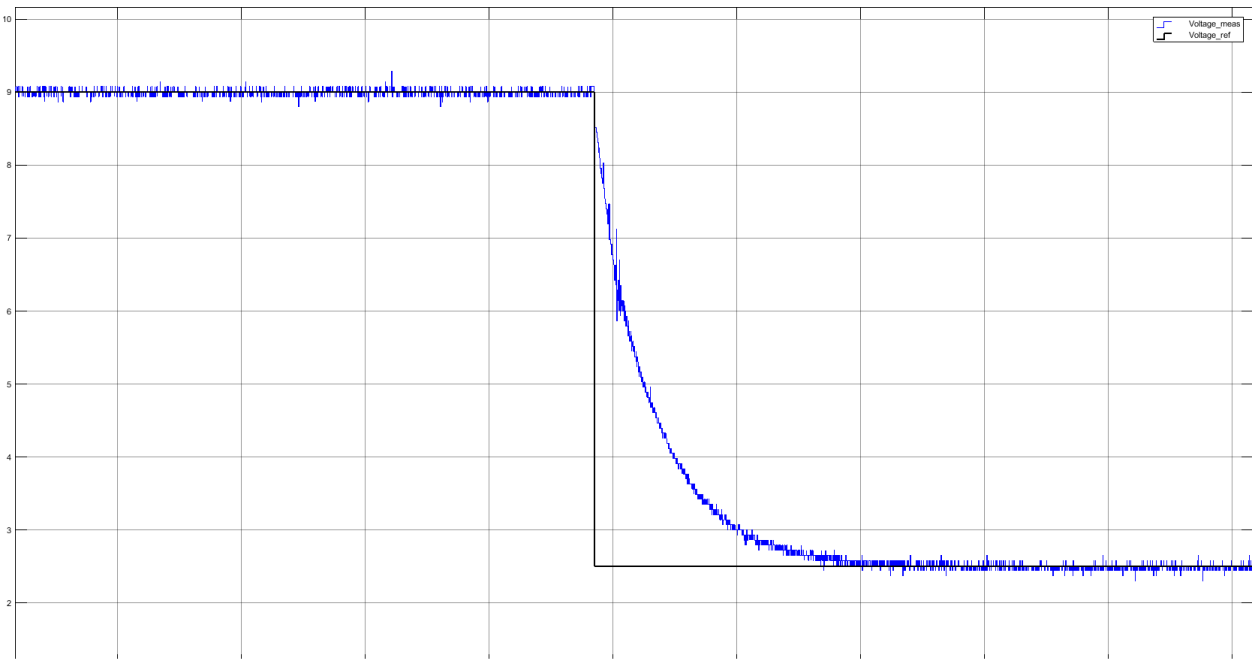

Figure 4-18 Step response of constant voltage regulation during buck mode (1 second per square)

5 Discussion

The purpose of the discussion chapter is to evaluate the chosen method, the chosen sources of information, the results and the overall project. During the ten weeks of the project many changes occurred because of different reasons, these will be discussed. A discussion of the project from an ethical point of view is also provided.

5.1 Result

In chapter result contains the consequences from the method in an objective manner. These results will be discussed and analyzed.

5.1.1 Simulations

The results from simulations contains figures with the calculated values from the method. The simulation in Simulink shows that the topology is suited for our application. The calculated value of 42 µH for the inductor concludes in small ripple of only 2 A. The capacitor decreases both the current and voltage ripple even further this is very promising for improving the battery lifespan. A smaller ripple also means that the computing of current RMS will be simpler.

The results from the simulations in MultiSIM were focused on the properties and characteristics of the MOSFET. The simulations show that considerations have been made to prevent false turn-on and overvoltage. The rise and fall time for the MOSFET provided in the result is sufficient for our application with a switching frequency of 50 kHz and a voltage gain of four.

5.1.2 Software

The software results indicate that the PI regulator can achieve constant current and constant voltage for both buck and boost mode, however further improvement is possible. With more time and effort better values for the PI coefficients can be found and a more accurate current sensor can be used to increase stability. Due to time limitations this was not in the scope of this project, however improvements can be implemented in the future. It should be noted that the Arduino will use computing power during continuous simulation mode with Simulink for communication which is detrimental to the test bench results. The software can definitely be further optimized.

5.1.3 Efficiency

The part about efficiency can be criticized since it is not guaranteed that the efficiency is the same for all power levels. It is also hard to say if the proposed design for the PCB could reach the same efficiency since the calculations for power losses are simplified.

5.1.4 PCB

The final results of the PCB design in Ultiboard shows that the PCB is shared between the DC/DC converter and the BLDC-inverter. The decision to do this was that this opened the possibility of sharing a single 475 µF capacitor on the 48 V DC bus of both the motor inverter and the DC/DC converter. This would minimize the risk oscillations that could occur with two systems connected to the 48 V battery with long cables. The shared PCB also makes the system more compact and easier to implement on the yacht.

The results were heavily affected by time limitations since only a proposed design of the PCB is provided and not an actual analysis of the created PCB. This means that the results only rely on the simulations results and results from the test bench. In turn, this can be criticized since the chosen components cannot be analyzed and a conclusion about the performance cannot be drawn.

5.2 Method

The used method in this project will both be discussed and criticized to defend and explain why different decisions were made.

5.2.1 Pre-study

The test case in the energy calculations uses values that are approximated so it should be noted that it is possible if for example more power is generated than consumed the power conversion might be turned off in the actual system. It also suggests a simple energy transfer strategy, but no evaluation of an implementation has been made on this because of time limitations.

The pre-study only compares two topologies that were analyzed amongst the many more that might do the job, however due to time limitations the more common full-bridge and half-bridge topologies were chosen for comparison.

5.2.2 Simulation

It should be kept in mind that the simulation in the method is not guaranteed to perfectly represent the real situation. Especially the simulation in Simulink that consider the components to be ideal, however it works well as a proof of concept since these simulations focus on control dynamics where the fast switching can be considered as ideal. The simulations in MultiSIM was improved in this manner due to the produced models by the manufacturers.

5.2.3 Components and Design

Many of the chosen components were chosen due to circumstances and limitation. A project stretched over 10 weeks implies a limitation to the number of components that can be analyzed and chosen between.

The method of choosing to build the inductor and wind it by hand can be criticized since the component might not work exactly as intended. The margin of error can be considered to be larger when the component is not thoroughly tested before use. This was however a consequence of the limitations due to the available suppliers not stocking a suitable inductor and having a custom-made being too expensive.

The decision of having the inductor outside of the PCB was due to the possibility of lowering the temperature on the PCB by using a separate heatsink for the inductor. To place the inductor outside of the PCB was also to minimize the noise and interference from the large magnetic field of the inductor.

The heat sink was designed for an ambient temperature of 30 ℃ which will not always be the case, since the system is implemented on a boat in a box that might have a different

temperature rise. It is also not taken into consideration how much the power dissipation from the inductor will affect the ambient temperature.

5.2.4 Software test

In order to test the software, we chose to use Simulink in combination with Arduino. As discussed earlier, this requires extra computing power by the Arduino which therefore affects the test but is taken into consideration. This method was chosen to test the software functions of constant voltage and constant current.

5.2.5 Chosen references

The majority of theory in this project is mostly based on [5] which is a book written by N. Mohan., T. M. Undeland and W. P. Robbins. The book covers a wide range of topics concerning power electronics for educational purposes and has withstood the test of time since it is considered by many to be a reliable source of information. This book provides both the theory behind power electronics as well as explaining implementation and design. [2] is a newer book by N. Mohan that contains more basic explanations that has been used to compliment [5]. The theory about MOSFETs are covered by [4] a book written by Baliga Jayant B. who is a well-known figure because of his involvement in the field of transistors. The book contributes to a more in-depth theory and understanding about transistors to support the explanation. The understanding of batteries and PV panels was provided by [8] which is a book written by Mertens K. in 2014. This book is newly written and up to date with subjects considering renewable energy.

The references used for comparison of different topologies was from IEEE database that contains reviewed papers from conferences and journals. Only papers written after 2010 was used to insure the reliability. During the design and choosing of components most of the information was given by the component datasheets. Application notes were also used to provide calculations of components surrounding the IC. Sources such as this can be criticized since the manufacturer might be biased towards their own product. But at the same time the manufacturer wants to provide good and accurate information about how their products should be used and designed to seem trustworthy.

5.3 Ethical Analysis

To evaluate the possible consequences of this thesis, an ethical analysis has been made. Power converters are only a part of the development of renewable energy. In order for the ethical analysis to be more specific, the consequences of an expansion of electrical boats for personal use was analyzed instead. The analysis followed the method ethical technology evaluation made by Sven-Ove Hansson at KTH Royal Institute of Technology. A summary from the proposed assessment schedule for the ethical technology evaluation is provided [27]. The technology development will also be analyzed with a precautionary principle in order to see if it appropriate to limit the development.

When evaluating the increased use of electrical boats there are many things to consider. The transformation from fossil fueled engines to electrical motors could be beneficial for the environment and the living conditions for fish but this implies the use of green energy. If the electricity is produced by oil and coal it is not certain that it is better for the environment. However, if the electrical boats would run on green energy the second issue is the construction of batteries. As it is today the construction of batteries that contain cobalt such as lithium-ion batteries affect both the environment and the people extracting it in a negative

manner. However, the development and knowledge about batteries is increasing and hopefully is a solution to that problem will be found.

To enforce this change, campaigns such as the one mentioned in the background might be needed to speed up the process. To compare with the electrical car the big change came when the company Tesla made big investments to speed up this process and to produce their own electrical cars. A change like that and further development of PV panels might be the condition for a rapid change to help our environment and lower the carbon emissions.

6 Conclusions

In this study, a design was suggested for a synchronous bidirectional half-bridge buck-boost converter used in a dual battery application. A software required to control it has been proposed as well as a design for a PCB implementation. Suggested components and thermal considerations were also made for the design of 40 A charge capability. A strategy for energy transfer seen in Figure 3-3 has been proposed but not evaluated due to time limitations. In the results, the simulations show that the converter design can work as means of bidirectional energy transfer. This was tested by using a test-bench which shows that the software is capable of controlling the converter to achieve constant current and constant voltage during both buck and boost mode.

For future work this system could be tested using a manufactured PCB that can be implemented in a yacht to evaluate the performance and design choices. This would provide a possibility to carry out a field test that could better show what the actual power flow is to compare with the test case in the energy calculations. In addition, the software can be developed to improve the regulation during constant voltage and constant current. With more in-depth research of the chosen batteries, better charging and discharging techniques may be found. The hardware can be improved to allow a more accurate and complex calculation of the SoC to be implemented.

7 References

[1] Regeringskansliet, “Ny klimatsatsning - regeringen föreslår premie för elutombordare”, Regeringskansliet, April 2018. [Online]. Available: https://www.regeringen.se/pressmeddelanden/2018/04/ny-klimatsatsning---regeringen-foreslar-premie-for-elutombordare/. [Accessed: June 2018].

[2] Mohan N., “Power Electronics: a first course”, 1st edition, New Jersey:John Wiley & Sons; 2011.

[3] Chao K., Tseng M., Huang C., Liu Y. and Huang L., “Design and Implementation of a Bidirectional DC/DC Converter for Stand-Alone Photovoltaic Systems”, *International Journal of Computer, Consumer and Control*, Vol. 2, No.3, 2013.

[4] Baliga Jayant B. “Fundamentals of Power Semiconductor Devices”, 1st edition, New York: Springer US; 2008.

[5] Mohan N., Undeland T.M. and Robbins W.P., “Power Electronics, Converters, Applications, and design”, 3rd edition. New Jersey: John Wiley & Sons Ltd; 2003.

[6] Vishay, Device Appl. Note AN608A, pp. 1-6.

[7] Texas Instruments, Appl. Note SLVA535A, pp. 3-5.

[8] Mertens K. “Photovoltaics Fundamentals, Technology and Practice”, 1st edition, New Jersey: John Wiley & Sons Ltd; 2014.

[9] Baccouche I., Mlayah A., Jemmali S., Manai B. and Essoukri Ben Amara N., "Implementation of a Coulomb counting algorithm for SOC estimation of Li-Ion battery for multimedia applications," 2015 IEEE 12th International Multi-Conference on Systems, Signals & Devices (SSD15), Mahdia, 2015

[10] Qazi S., “Standalone Photovoltaic (PV) Systems for Disaster Relief and Remote Areas”, 1st edition, Amsterdam: Elsevier; 2016

[11] ON Semiconductor, Appl. Note AN-6076, pp.1-4.

[12] NASA (2017), “Engineering Design“, NASA, November 7, 2017. [Online]. Available: https://mynasadata.larc.nasa.gov/engineering-design/.[Accessed: June 2018]

[13] Ioinovici A., “Power electronics and energy conversion systems”, 1st edition, Chichester:John Wiley & Sons Ltd; 2013

[14] Yu Z., Kapels H. and Hoffmann K. F., “A Novel Control Concept for High-Efficiency Power Conversion with the Bidirectional Non-inverting Buck-Boost Converter”, *2016 18th European Conference on Power Electronics and Applications (EPE'16 ECCE Europe),* Karlsruhe, 2016.

[15] Ouchi T., Kanouda A., Takahashi N. and Moteki M. , "Seamless controlled parallel bi-directional DC/DC converter for energy storage system" *2014 16th European Conference on Power Electronics and Applications*, Lappeenranta, 2014

[16] Xu X., Zheng C., Hu C., Lu Y. and Wang Q., "Design of Bi-directional DC/DC converter," *2016 IEEE 11th Conference on Industrial Electronics and Applications (ICIEA)*, Hefei, 2016

[17] Infineon, "OptiMOS™ 5 Power-Transistor 150V", IPB044N15N5 datasheet, April 2016 [Revised April 2016].

[18] Texas Instruments, "Single-Channel Isolated Gate Drivers" UCC5390SC datasheet, June 2017 [Revised May 2018].

[19] Texas Instruments, "Switched-Capacitor Voltage Converters With Regulators" LT1054 datasheet, Feb. 1990 [Revised July. 2015].

[20] Allegro, Appl. Note A3946, pp.7-9.

[21] Vishay, "Long Side Termination Thick Film Chip Resistors" RCL e3 datasheet, Feb. 2017 [Revised July. 2017].

[22] Comchip, "SMD Schottky Barrier Rectifiers" CDBC5150-HF datasheet [Rev.B].

[23] TDK, "Ferrites and accessories" SIFERRIT material N27 datasheet, May. 2017 [Revised May 2017].

[24] CircuitCalculator.com, "PCB Via Calculator", CircuitCalculator.com, Mars, 2006. [Online]. Available: http://circuitcalculator.com/wordpress/2006/03/12/pcb-via-calculator/ [Accessed: June 2018].

[25] CircuitCalculator.com, "PCB Trace Width Calculator", CircuitCalculator.com, January, 2006. [Online]. Available http://circuitcalculator.com/wordpress/2006/01/31/pcb-trace-width-calculator/ [Accessed: June 2018].

[26] Atmel, "SMART ARM-based MCU" SAM3X8E ARM Cortex-M3 datasheet, Feb. 2017 [Revised Mars 2015].

[27] Hansson S. O., "Teknik och etik", KTH University Philosophy department, 2009.

8 Appendix

8.1 Batteries Used in Project

8.1.1 12 V lead-acid battery

Existing in the boat is a set of four parallel 12 V VRLA batteries. The batteries are of the type PartSmart Maringel MG3120. The table below is summarizing the battery data:

		Unit	Bank
Nominal voltage	V	12	12
Max voltage	V	14.4	14.4
Rated capacity	Ah	96	384
Maximum DoD	%		60
Stored energy	Wh		2765
Max charging current	A		38
Recommended charge current	A	9.6	
Recommended charge voltage	V	14.4-14.6	

8.1.2 48 V LiFePo4 battery

The 48 V battery system is based on LiFePo4 high power cells from EV (GWL) Power. The battery bank is built by 16 series connected 3.2 V, 60 Ah cell modules. A battery management system from EV-Power will be used which includes balancing between cells as well as isolating contactors, protecting from over charging and deep discharge. The depth of discharge is limited to 75%.

No of cells		16
Q	Ah	60
I_{max}	A	180
U_{nom}	V	51.2
U_{max}	V	60.8
U_{min}	V	40
Ri	Ω	0.032
W_{bat}	Wh	2304
Weight	kg	27
Volume	l	15

8.2 PV panels used in project

There are two PV panels that will be used to generate power to the 12 V battery. The specifications for standard test conditions are written below.

PV1

- Name: Solara SM 160 M
- Pmax: 40 W
- Umax: 16.7 V
- Imax: 2.2 A

PV2

- PPAM Onyxium 145W
- Pmax: 144 W
- Umax 16.62 V
- Imax: 8.64 A